Fully nonlinear solitary waves in continuously stratified incompressible Boussinesq fluids

David J. Brown and Douglas R. Christie

Citation: Physics of Fluids **10**, 2569 (1998); doi: 10.1063/1.869771
View online: http://dx.doi.org/10.1063/1.869771
View Table of Contents: http://scitation.aip.org/content/aip/journal/pof2/10/10?ver=pdfcov
Published by the AIP Publishing

Fully nonlinear solitary waves in continuously stratified incompressible Boussinesq fluids

David J. Brown[a] and Douglas R. Christie
Research School of Earth Sciences, Australian National University, Canberra ACT 0200, Australia

(Received 9 May 1997; accepted 6 July 1998)

This study is concerned with a fully nonlinear theoretical treatment of internal solitary waves in continuously stratified, incompressible, inviscid, shear-free Boussinesq fluids. Results are presented for wave propagation in both deep and shallow fluids with four different ambient stability profiles. Only the dominant mode with the greatest wave speed is considered. The morphology of finite-amplitude internal solitary waves in Boussinesq fluids is shown to be very sensitive to the precise form of the stability profile. The calculations indicate that a wave of maximum amplitude, which is less than the total fluid depth, exists for all internal solitary waves in continuously stratified Boussinesq fluids of finite depth. There is apparently no upper limit on the amplitude of internal solitary waves in many physically realistic unbounded fluids. Large amplitude waves of this type are mutually similar in form and the morphology of these waves appears to be independent of the ambient stability profile in the waveguide layer. It is shown that the properties of highly nonlinear waves with recirculating flow depend on the density distribution and vorticity of the trapped fluid inside the closed circulation cell. Fluid velocity components associated with the wave motion are evaluated and used to calculate the surface perturbation pressure. The surface perturbation pressure signature for internal solitary waves is found to change with the onset of recirculation from a single-crested profile at small wave amplitudes to a bimodal profile at large wave amplitudes. Results for solitary waves in finite-depth fluids differ from those found for deep fluids in that the surface perturbation pressure at the center of the wave eventually changes sign as wave amplitude increases. © *1998 American Institute of Physics.* [S1070-6631(98)02310-1]

I. INTRODUCTION

The theory of highly nonlinear internal propagating waves in stably stratified incompressible fluids has received relatively little attention compared with work on large amplitude surface waves. This is surprising since internal waves of large amplitude are known to occur commonly in both the oceans (see, e.g., Ostrovsky and Stepanyants[1]) and the lower atmosphere (Christie[2]). This paper will be concerned with a general theoretical description of highly nonlinear internal solitary waves in incompressible, continuously stratified Boussinesq fluids.

The theoretical approach which is used to study internal waves of arbitrary amplitude is often determined by the characteristics of the flow configuration. The investigation of large amplitude wave motions in fluids with a sharp interface is usually carried out using boundary integral techniques. Numerical solutions for fully nonlinear solitary waves at the interface between two incompressible fluids of differing but constant density have been studied in considerable detail by Pullin and Grimshaw[3] using a boundary integral equation formulation with conformal mapping. An interesting extension of this work on the two-fluid problem has been given by Forbes and Belward,[4] who calculate the properties of large amplitude waves at the interface between a lower layer of incompressible irrotational fluid of constant density and an unbounded compressible upper layer in which the density decreases exponentially with height.

A different theoretical approach is usually used to study waves of finite amplitude in continuously stratified, incompressible, inviscid fluids. In this case, waves of arbitrary amplitude are described by solutions of the Dubreil-Jacotin–Long (DJL) equation (Dubreil-Jacotin;[5] Long[6]), a nonlinear elliptic eigenvalue problem for the streamfunction with simple boundary conditions. There is now an infinite sequence of internal wave modes, $n=1,2,...$, where the lowest mode ($n=1$) is the fastest propagating mode and each mode has n extrema in the interior of the fluid. Numerical solutions of the DJL equation have been presented by a number of authors. Davis and Acrivos[7] calculated mode-2 solitary wave solutions in the Boussinesq approximation for waves in a thin pycnocline with constant Brunt–Väisälä frequency, N, embedded in a neutrally stable unbounded fluid. These authors showed that regions with closed circulation exist in solitary waves of large amplitude in agreement with laboratory observations. Tung *et al.*,[8] in a very detailed study, have presented the results of numerical calculations for solitary wave propagation in both deep and shallow shear-free Boussinesq fluids with a $\mathrm{sech}^2(z)$ Brunt–Väisälä frequency distribution. The large amplitude mode-2 solitary wave solutions obtained by Tung *et al.* also exhibit regions of recirculating fluid. In addition, these authors show that the wavelength of internal solitary waves eventually increases with

[a]Corresponding author. Current address: Center for Monitoring Research, 1300 North 17th Street, Arlington, VA 22209.

increasing amplitude in contrast with the predictions of weakly nonlinear theory. A very elegant iterative algorithm, which is based on a variational technique, has been developed by Turkington *et al.*[9] and used to calculate the streamline pattern of mode-1 internal solitary waves in both shallow and relatively deep continuously stratified fluids. The propagation of large amplitude internal waves has also been studied by Vanden-Broeck and Turner.[10] These authors used finite difference techniques in conjunction with a boundary integral method to determine solutions of the DJL equation for periodic waves in a non-Boussinesq fluid with upper and lower layers of constant density separated by a layer in which the fluid density varies continuously. The solutions found by these authors show that ''generalized'' internal nonlinear waves exist in the form of primary mode-2 waves with a superimposed stationary train of smaller amplitude mode-1 waves. It is worth noting as well that large amplitude internal solitary wave solutions have been found (Benney and Ko;[11] Benney and Grimshaw;[12] see also Derzho and Velarde[13]) in the Boussinesq approximation using asymptotic expansion techniques which are similar to those used in the development of weakly nonlinear wave theory. Finally, in a recent study which has some bearing on the present investigation, Derzho and Grimshaw[14] utilize the solitary wave solutions of an approximate form of the DJL equation, valid in cases of weak stratification, to examine the properties of solitary waves in shallow weakly stratified fluids. The distinguishing feature of their work is that these authors show that by matching inner- and outer-solutions, and assuming constant density in the inner region, it is possible to maintain a vortex core of fluid, which to leading order is stagnant. A necessary condition of this construction, however, is that the density and vorticity be discontinuous across the core boundary.

Much to the chagrin of experimentalists, there has until now, been a comparative dearth of theoretical results concerning the influence of the stability profile on the properties of highly nonlinear internal solitary waves. Addressing this particular problem forms the focus of the present investigation. In this study, the properties of solitary waves propagating in fluids with a wide variety of realistic stability profiles are examined. This work thus forms a firm foundation for the interpretation of experimental observations of internal solitary waves. Further, since solitary wave observations in geophysical environments are almost entirely limited to mode-1 waves, only the dominant first mode with the greatest wave speed will be considered in this investigation. Calculations will also be presented which illustrate the fluid velocity components and surface perturbation pressure profiles for solitary waves in both deep and shallow fluids. These calculations can be used to interpret observations of atmospheric solitary wave phenomena. A new derivation of the Dubreil-Jacotin–Long equation, which avoids the restriction on waves with regions of recirculating flow that appears in other derivations, is presented in Sec. II. Section III is devoted to a detailed study of the numerical solutions of the DJL equation which illustrate the influence of the stability profile on the properties of highly nonlinear solitary waves in both shallow and deep fluids. In Sec. IV we present the results of a detailed investigation of the influence of the properties of trapped recirculating fluid on the morphology of large amplitude waves. Calculations of fluid velocity components and surface perturbation pressures are presented in Sec. V and the significance of our results and their relevance to the interpretation of experimental observations are summarized in Sec. VI. A novel numerical technique, which provides very accurate results, has been developed to determine the solutions of the Dubreil-Jacotin–Long equation. An outline of this algorithm is presented in the Appendix.

II. THE GOVERNING EQUATION FOR NONLINEAR WAVES IN CONTINUOUSLY STRATIFIED FLUIDS

All of the derivations of the Dubreil-Jacotin–Long equation which have been reported in the literature (see, e.g., Dubreil-Jacotin,[5] Long,[6] Benjamin,[15] and Benney and Ko[11]) have been based on the assumption that the total streamfunction for stationary flow, ψ, as defined in terms of the relative fluid velocities $u_r=\partial\psi/\partial z$ and $w_r=-\partial\psi/\partial x$ in the horizontal and vertical directions, respectively, varies monotonically with z throughout the fluid domain. That is, it is assumed that closed circulation does not occur at any point in the fluid. This would appear to limit the use of the Dubreil-Jacotin–Long equation to the description of stationary flows in fluids where all streamlines are connected to the upstream flow. It is clear, however, that this condition may be unnecessarily restrictive. Large amplitude solitary wave solutions to this equation have been found (Davis and Acrivos,[7] Tung *et al.*[8]) with recirculating flow. These solutions appear to describe, at least qualitatively, the laboratory observations of Davis and Acrivos,[7] Maxworthy,[16] and Stamp and Jacka[17] and observations of large amplitude solitary waves in the lower atmosphere with regions of trapped recirculating fluid (see, e.g., Doviak *et al.*[18]). This suggests that the Dubreil-Jacotin–Long equation may indeed describe solitary waves with recirculating eddies, at least over time scales during which the influence of viscous forces can be neglected. It is known that viscous forces will eventually alter the flow pattern in closed streamline regions.[19] It is also worth noting at this point that the variational treatment of the highly nonlinear internal wave problem as described by Turkington *et al.*[9] is not restricted to a description of stationary wave motions in which all streamlines connect to the upstream flow. We therefore present here a brief outline of a more general derivation procedure for the Dubreil-Jacotin–Long equation which allows recirculation in the streamline flow pattern.

Consider two-dimensional steady wave propagation in an incompressible, shear-free stably stratified, inviscid, nondiffusive fluid in which the density, $\rho(\psi)$, is constant along a streamline. The kinetic energy density $\mathscr{T}$ associated with the wave motion is given by $\mathscr{T}=\frac{1}{2}\rho(\psi)\{(\psi_z-c)^2+\psi_x^2\}$, and the gravitational potential energy density $\mathscr{V}$ at any point in the flow field is determined by $\mathscr{V}=-g\int_z^{\psi/c}\{\rho(\psi)-\rho(z'c)\}dz'$. Here, g is the acceleration due to gravity, c is the wave speed, and the upper limit to the integral, ψ/c, in the expression for $\mathscr{V}$ corresponds to the ''zero'' point of the

potential, i.e., the point where the restoring force due to buoyancy vanishes.

The Euler–Lagrange equation for the Lagrangian density $\mathscr{L}=\mathscr{T}-\mathscr{V}$ is

$$\frac{\partial}{\partial x}\left(\frac{\partial \mathscr{L}}{\partial \psi_x}\right)+\frac{\partial}{\partial z}\left(\frac{\partial \mathscr{L}}{\partial \psi_z}\right)-\frac{\partial \mathscr{L}}{\partial \psi}=0.$$

We note that

$$\frac{\partial \mathscr{L}}{\partial \psi}=\frac{1}{2}\frac{d\rho}{d\psi}\{(\psi_z-c)^2+\psi_x^2\}-g\int_{\psi/c}^{z}\left\{\frac{\partial \rho(\psi)}{\partial \psi}-\frac{\partial \rho(z'c)}{\partial \psi}\right\}dz'$$

$$=\frac{1}{2}\frac{d\rho}{d\psi}\{(\psi_z-c)^2+\psi_x^2\}-g\,\frac{d\rho(\psi)}{d\psi}\left(z-\frac{\psi}{c}\right),$$

$$\frac{\partial \mathscr{L}}{\partial \psi_x}=\rho(\psi)\psi_x,$$

and

$$\frac{\partial \mathscr{L}}{\partial \psi_z}=\rho(\psi)(\psi_z-c).$$

Hence,

$$\frac{\partial}{\partial x}\left(\frac{\partial \mathscr{L}}{\partial \psi_x}\right)=\frac{d\rho}{d\psi}\,\psi_x^2+\rho\psi_{xx},$$

$$\frac{\partial}{\partial z}\left(\frac{\partial \mathscr{L}}{\partial \psi_z}\right)=\frac{d\rho}{d\psi}\,\psi_z(\psi_z-c)+\rho\psi_{zz}.$$

Thus, the Euler–Lagrange equation for $\mathscr{L}$ can be written as

$$\rho\nabla^2\psi+\frac{d\rho}{d\psi}\{\psi_x^2+\psi_z^2-\psi_z c\}-\frac{1}{2}\frac{d\rho}{d\psi}\{(\psi_z-c)^2+\psi_x^2\}+g\,\frac{d\rho}{d\psi}\left(z-\frac{\psi}{c}\right)=0,$$

which can be rearranged to give the usual form of the Dubreil-Jacotin–Long equation:

$$\nabla^2\psi+\frac{1}{\rho(\psi)}\frac{d\rho}{d\psi}\left\{\frac{(\nabla\psi)^2-c^2}{2}+g\left(z-\frac{\psi}{c}\right)\right\}=0. \tag{1}$$

This particular derivation is not restricted to the description of stationary flows in which all streamlines connect to the upstream flow. In addition, this Lagrangian derivation is physically more fundamental than the momentum equation approach because it follows directly from an action principle.

Consider, now, a fluid in which the ambient density stratification is given by $\rho(\psi)=\rho_0(1-\sigma F(\psi))$, where F is a monotonically increasing function and σ is the Boussinesq parameter. The DJL equation can then be written (see, e.g., Tung *et al.*[8]) in terms of the perturbation streamfunction, $\phi=\psi-z$, as

$$\nabla^2\phi+\frac{F'(\phi+z)}{1-\sigma F(\phi+z)}\left[\Lambda\phi-\frac{\sigma}{2}(\phi_x^2+\phi_z^2+2\phi_z)\right]=0, \tag{2}$$

where all variables are nondimensional and the eigenvalue, Λ, is given by $\Lambda=\sigma g h/c^2$. We note that $\psi=z$ in the undisturbed flow ahead of the wave. The eigenvalue, Λ_0, corresponding to the linear wave limit is defined by $\Lambda=\Lambda_0 c_0^2/c^2$ where c_0 is the linear wave speed. In the Boussinesq approximation, contributions to the wave inertia obtained directly from variations in the ambient density profile are ignored. A statement of the Boussinesq approximation in the present context, therefore, is equivalent to assuming that σ in Eq. (2) can be ignored, except where it enters the equation through Λ. Hence, in the Boussinesq approximation, the DJL equation takes the much simpler form

$$\nabla^2\phi+\Lambda F'(\phi+z)\phi=0. \tag{3}$$

The boundary conditions on ϕ for internal solitary wave motions are

$$\text{(i)}\quad \phi(0)=0, \tag{4}$$

$$\text{(ii)}\quad \phi(H)=0, \tag{5}$$

and

$$\text{(iii)}\quad \lim_{x\to\pm\infty}\phi=0. \tag{6}$$

As in previous studies of the solutions of the Dubreil-Jacotin–Long equation (Davis and Acrivos;[7] Tung *et al.*[8]), we shall assume that $\rho(\psi)=\rho_0(1-\sigma F(\psi))$ is valid for both positive and negative values of ψ unless noted otherwise.

III. PROPERTIES OF FULLY NONLINEAR SOLITARY WAVES IN BOUSSINESQ FLUIDS

This paper is primarily concerned with the influence of the density profile, $\rho(\psi)$, in the ambient fluid on the properties of highly nonlinear internal waves. Thus, attention will be focused on four different stability profiles:

Case 1: $F(\psi)=\tanh(\psi)$,	$N^2(\psi)$, varies as $\mathrm{sech}^2(\psi)$;
Case 2: $F(\psi)=(1-e^{-\psi})$,	$N^2(\psi)$ varies as $e^{-\psi}$;
Case 3: $F(\psi)=2/\pi\ \arctan(\psi)$,	algebraic Brunt–Väisälä frequency profile;
Case 4: $F(\psi)=\psi/\psi+1$,	algebraic Brunt–Väisälä frequency profile.

Plots of the Brunt–Väisälä frequency and density as a function of height for these various stability profiles are illustrated in Fig. 1.

Laboratory investigations of solitary wave motions in continuously stratified fluids often use ambient fluids with densities that are well described by the density profile considered in *case 1* (see, e.g., Ref. 17). The second group of ambient density profiles are considered because non-Boussinesq flows with these ambient density profiles may provide a first-order model for large scale wave motions in a (nonrotating) atmosphere. Although we are considering only Boussinesq flows here, many of the wave properties may carry over to the non-Boussinesq regime. In the last two cases, the properties of solitary waves in fluids with algebraic Brunt–Väisälä frequency profiles are examined. By comparing the properties of solitary waves propagating in *case 1* fluids with those of solitary waves propagating in the *case 3*

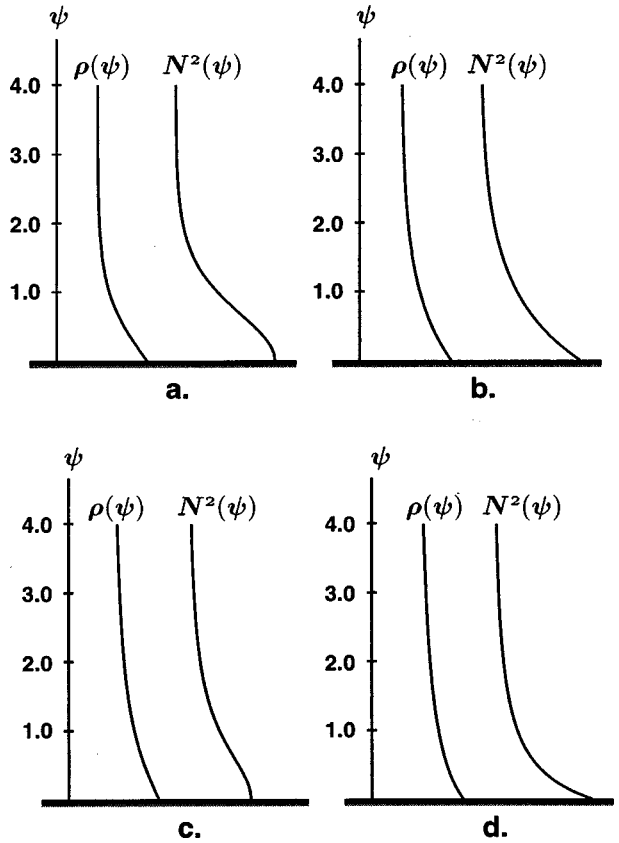

FIG. 1. Ambient fluid density, $\rho(\psi)$, and Brunt–Väisälä frequency, $N^2(\psi)$, profiles studied in this investigation: (a) $\rho(\psi)=\rho_0(1-\sigma\tanh(\psi))$; (b) $\rho(\psi)=\rho_0(1-\sigma(1-e^{-\psi}))$; (c) $\rho(\psi)=\rho_0(1-\sigma(2/\pi)\arctan(\psi))$; (d) $\rho(\psi)=\rho_0(1-\sigma\psi/(\psi+1))$.

fluids, important conclusions can be inferred concerning the nature of solitary waves of large amplitude in general. Solitary waves propagating in fluids with an ambient Brunt–Väisälä frequency profile described in *case 4* will be only briefly considered. Although a little unphysical, the main reasons for the inclusion of this density profile is to establish the properties of these solitary waves prior to the density profile extension considered in Sec. IV.

Values of Λ_0 have been evaluated for each of these flow models from numerical solutions of the vertical modal equation $\varphi_{zz}+(N^2/c_0)\varphi=0$ subject to the appropriate boundary conditions for finite depth fluids $[\varphi(0)=0,\ \varphi(H)=0]$ or unbounded fluids $[\varphi(0)=0,\ \lim_{z\to\infty}\varphi_z=0]$. These values are listed in Table I.

A brief outline of the novel finite-difference technique which is used to find the solitary wave solutions of the Dubreil-Jacotin–Long equation is given in the Appendix. Numerical solutions of (3) have been found for each density profile for both weakly nonlinear and highly nonlinear waves in fluids with total nondimensional fluid depths in the range from $H=1$ to $H=200$. The computational domain for all calculations is chosen to be sufficiently wide such that the solution is not noticeably changed by a further increase in domain width. For computational expediency, the results described here are restricted to solitary waves which are symmetrical about $x=0$.

The definition of wave amplitude we will be assuming throughout the remainder of this paper is the displacement, $\eta_{\max}$, of the streamline with maximum displacement. The wavelength we will be assuming (unless otherwise noted in the text) will be the full-width at half-maximum amplitude, $\mathscr{W}_{1/2}$ of the streamline on which ψ takes the value 1.0.

We will now examine the influence of the ambient density profile on the morphology and propagation characteristics of solitary internal waves in Boussinesq fluids.

A. Case 1: $\rho(\psi)=\rho_0(1-\sigma\tanh(\psi))$

Highly nonlinear mode-2 solitary waves in Boussinesq fluids with $F(\psi)=\tanh(\psi)$ have been studied in considerable detail by Tung *et al.*[8] Here, we extend the work of these authors to higher wave amplitudes and to a wider range of total fluid depths. The mode-1 solitary wave calculations were carried out in a computational domain with a lower rigid boundary. The results of these calculations are entirely equivalent to the mode-2 results obtained by Tung *et al.* because the region above the plane of symmetry in the mode-2 flow domain used by Tung *et al.* is dynamically similar to the region below the plane of symmetry in the Boussinesq approximation. Examples of typical relative streamline patterns for small and large amplitude solitary waves in this flow configuration are shown in Fig. 2. The results displayed in Fig. 2(b) for a large amplitude solitary wave are in agreement with the calculations described by Davis and Acrivos[7] and Tung *et al.*,[8] which show that large amplitude solitary wave solutions of the Dubreil-Jacotin–Long equation may exhibit regions of trapped recirculating fluid.

Plots of wave amplitude, $\eta_{\max}$, as a function of the eigenvalue, Λ, are displayed in Fig. 3 for various values of the total nondimensional fluid depth in the range from $H=1$ to $H=200$. A comparison of the results in Fig. 3 with the plots of $(-\phi)_{\max}$ versus the eigenvalue given in Fig. 14 of Tung *et al.*[8] shows that our calculated results are almost identical to those found by Tung *et al.* in the parameter range where the calculations overlap. The one area where these results differ is in the neighborhood of the point corresponding to the minimum value of Λ. The calculations presented by Tung *et al.* indicate that the solution curve varies continuously between the lower solution branch and the upper solu-

TABLE I. Eigenvalues Λ_0 in the linear wave limit.

H	1	2	4	7.5	10	30	100	200	∞
$F(\psi)=\tanh(\psi)$	12.60	5.09	3.08	2.48	2.34	2.10	2.03	2.01	2.00
$F(\psi)=(1-e^{-\psi})$	15.84	6.03	3.04	2.12	1.91	1.58	1.48	1.46	1.44
$F(\psi)=\arctan(\psi)$	19.39	7.10	3.42	2.14	1.81	1.14	0.84	0.75	0.45
$F(\psi)=\psi/(\psi+1)$	20.79	8.42	4.06	2.40	1.97	1.09	0.71	0.60	0.30

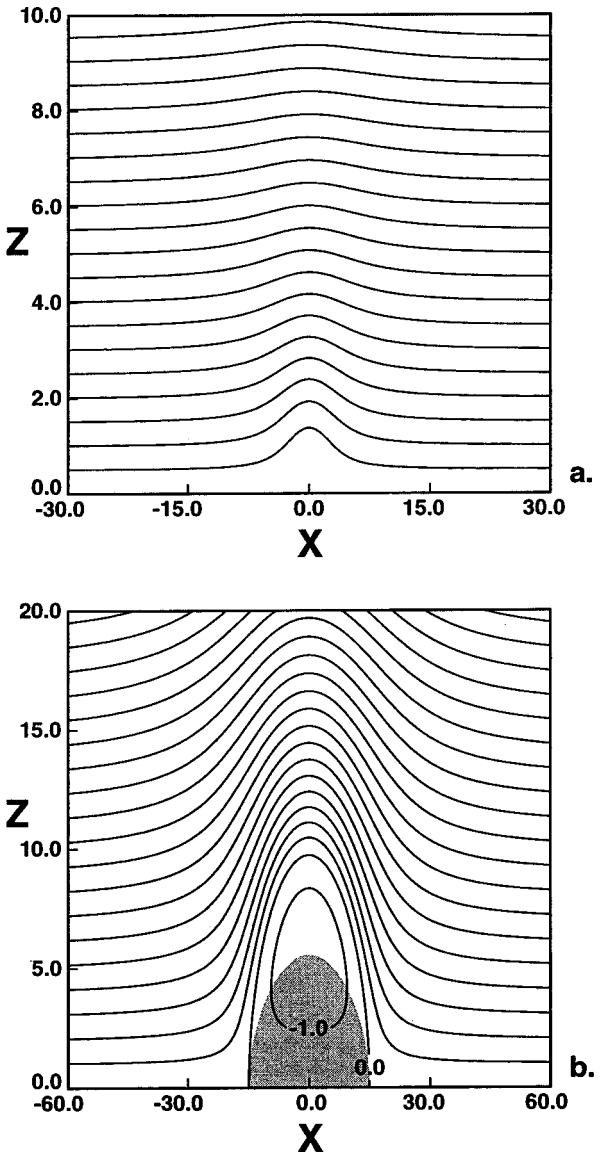

FIG. 2. Contour plots of the total streamfunction for small and large amplitude solitary wave solutions to the DJL equation for a deep, Boussinesq shear-free fluid with density $\rho(\psi)=\rho_0(1-\sigma\tanh(\psi))$ and $H=200$: (a) $a/h=0.92$; (b) $a/h=9.7$. Only the lower portion of the computational domain is illustrated. The shaded region corresponds to the area in the flow field where the horizontal particle velocity exceeds the speed of the wave.

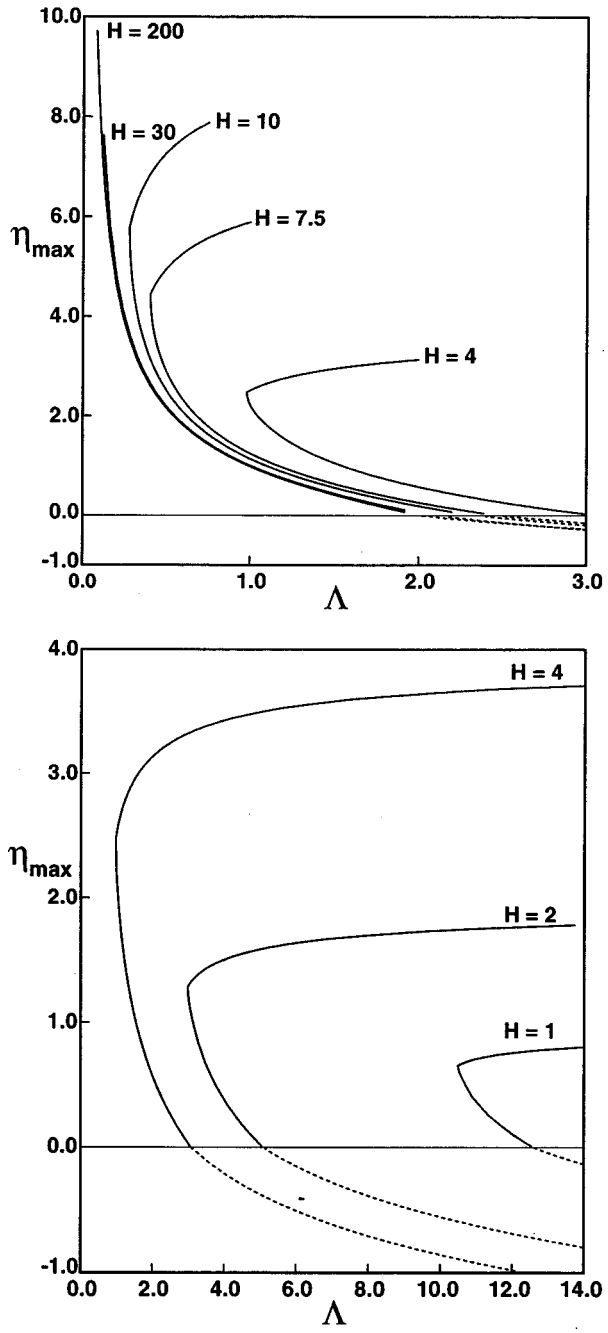

FIG. 3. Wave amplitude $\eta_{\max}$ vs eigenvalue Λ for flow models with density $\rho(\psi)=\rho_0(1-\sigma\tanh(\psi))$. The total nondimensional fluid depth H corresponding to each solution branch is indicated on the diagram. The dashed curve denotes subcritical stationary wave solution branches.

tion branch. In contrast to the results found by Tung *et al.*, our calculations clearly exhibit a discontinuity in the amplitude–eigenvalue curves for waves in finite-depth fluids at the limit point. It appears, at least to within the accuracy of our calculations, that $d\eta_{\max}/d\Lambda\to-\infty$ as $\eta_{\max}$ approaches the amplitude, η_0, at the limit point from below while $d\eta_{\max}/d\Lambda$ is positive, but finite, in the limit $\eta_{\max}\to\eta_0$ from above.

It has been noted by Stamp and Jacka (Ref. 17) that the presentation of theoretical results in a form such as that displayed in Fig. 3 which uses the eigenvalue Λ instead of the wave speed has led to some confusion in the literature when attempts are made to compare theoretical results with observed amplitude–speed curves. We will therefore, for the sake of clarity, present in Fig. 4 plots showing the functional dependence of amplitude on nondimensional wave speed, c/c_0, for the flow models used in Fig. 3. Values of the linear wave speed $c_0=\sqrt{\sigma gh/\Lambda_0}$ may be determined from the computed values for Λ_0 given in Table I.

We have carried out a detailed investigation of the unusual upper branch solutions in Fig. 3 which were first discovered by Tung *et al.*[8] In contrast to all solutions on the lower branch which have a uniquely defined wavelength, we have found that the wavelength of all upper branch solutions depends entirely on the width of the computational domain. This is illustrated in Fig. 5 by the solitary wave solutions

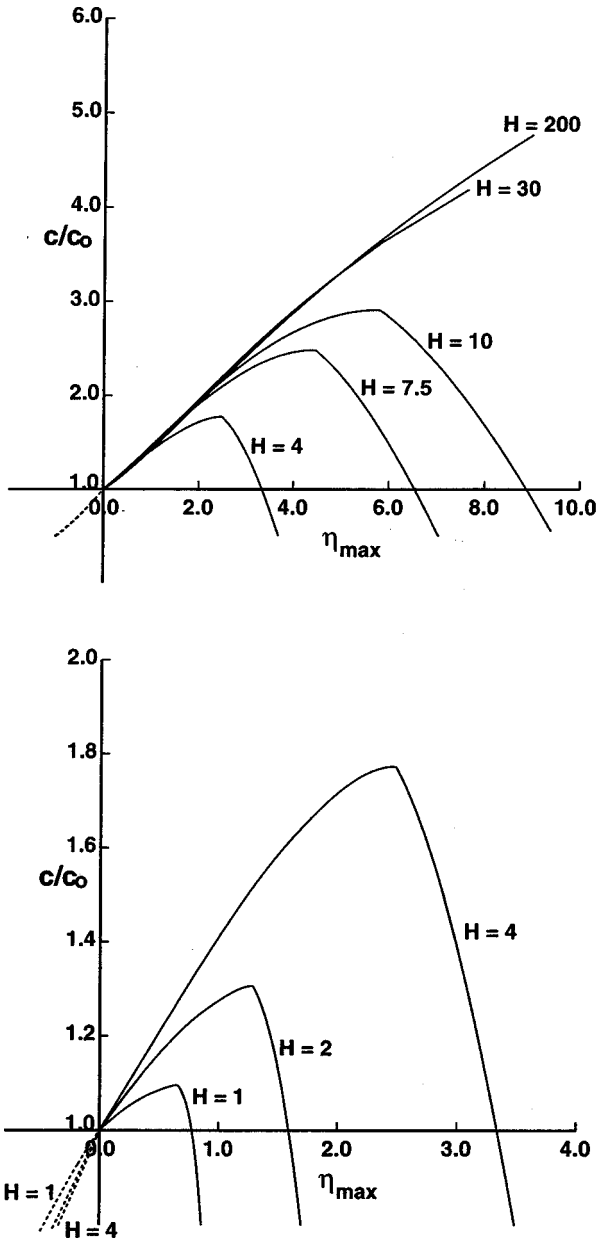

FIG. 4. Wave amplitude $\eta_{\max}$ vs nondimensional wave speed c/c_0 for flow models with density $\rho(\psi)=\rho_0(1-\sigma\ \tanh(\psi))$. The nondimensional total fluid depth H for each solution branch is indicated on the diagram. The dashed curve denotes subcritical stationary wave solution branches.

found for a fluid with $H=4$ and $\Lambda=0.981$ for total nondimensional computational domain widths of 40, 200, and 400. Thus, the wavelength of these unusual time-independent solutions can be arbitrarily large. It appears that all of these domain-width-dependent solutions have the same amplitude and the same shape near the horizontal boundaries of the domain provided the width of the domain is sufficiently large. Furthermore, the upper solution branch describes both supercritical ($c>c_0$) and subcritical ($c<c_0$) solitary waves in contrast with the lower branch solutions which are always supercritical. Indeed, it appears that the upper branch curves extend to $c=0$. These solutions also differ from the more familiar solitary wave solutions described by the lower solution branch in that the horizontal derivative of the streamlines which lie outside the closed circulation cell does not vanish at the domain boundaries for any computational domain width. Thus, these unusual solitary wave solutions to the boundary value problem defined by Eqs. (3)–(6) would not exist if an additional boundary condition, $\lim_{x\to\pm\infty}\phi_x=0$, is also included in the set of boundary conditions on ϕ. Finally, we note that upper branch solutions always exhibit recirculating flow. These properties suggest that the upper branch solutions may not represent physically realistic solutions. In any case, it is clear that a physically realistic solitary wave of maximum amplitude with a uniquely defined wavelength exists in Boussinesq fluids of finite depth with hyperbolic-tangent density profiles. This well-defined internal solitary wave also propagates with maximum speed.

We have also found a new and unusual class of solitary wave solutions which appear to be similar in many respects to the upper branch solutions. The eigenvalue–amplitude and amplitude–speed curves for these waves are denoted by the dashed curves in Figs. 3 and 4. These waves take the form of subcritical solitary waves of depression and again have wavelengths constrained only by the width of the computational domain [see Fig. 5(a)]. This class of wave has been found in the case of every other density profile, but are unphysical and so will not be considered further here.

The functional dependence of wave amplitude on wavelength is illustrated in Fig. 6 for the lower solution branch. These results are similar to those found by Tung *et al.*[8] In all cases, the wavelength decreases initially to a minimum value with increasing wave amplitude. The wavelength then increases with further increases in amplitude for waves in both deep and shallow fluids. It is worth noting that the onset of closed circulation is not an essential requirement for wave broadening. Our results, which are summarized in Table II, show that closed circulation always occurs at amplitudes which are significantly less than the amplitude corresponding to minimum wavelength.

The results presented in Figs. 3–5 for fluids with depth $H=200$ are almost indistinguishable from results computed for a total fluid depth of $H=100$. Hence, the $H=200$ results correspond essentially to a fluid of infinite depth. These deep fluid results are particularly interesting since they indicate that the wavelength of very large amplitude waves of this type varies linearly with wave amplitude. Thus, the wave profiles of these large amplitude deep-fluid waves differ only by a scaling factor and, in contrast with surface waves and internal waves in finite-depth fluids, there appears to be no upper limit to the amplitude of internal solitary waves in unbounded Boussinesq fluids. This behavior has been confirmed by further calculations (see Fig. 7) which extend the wave amplitude for the $H=200$ flow model to a dimensionless amplitude of about 30. These results suggest that in the large amplitude limit, the wavelength to amplitude ratio for solitary waves in unbounded fluids with a hyperbolic tangent density profile has a value of about 3.13.

Pullin and Grimshaw[3] have shown that large amplitude solitary waves on the interface between two unbounded Boussinesq fluids differ in shape only by a scaling factor. Thus, the results presented here extend the theoretical results of Pullin and Grimshaw to Boussinesq fluids with continu-

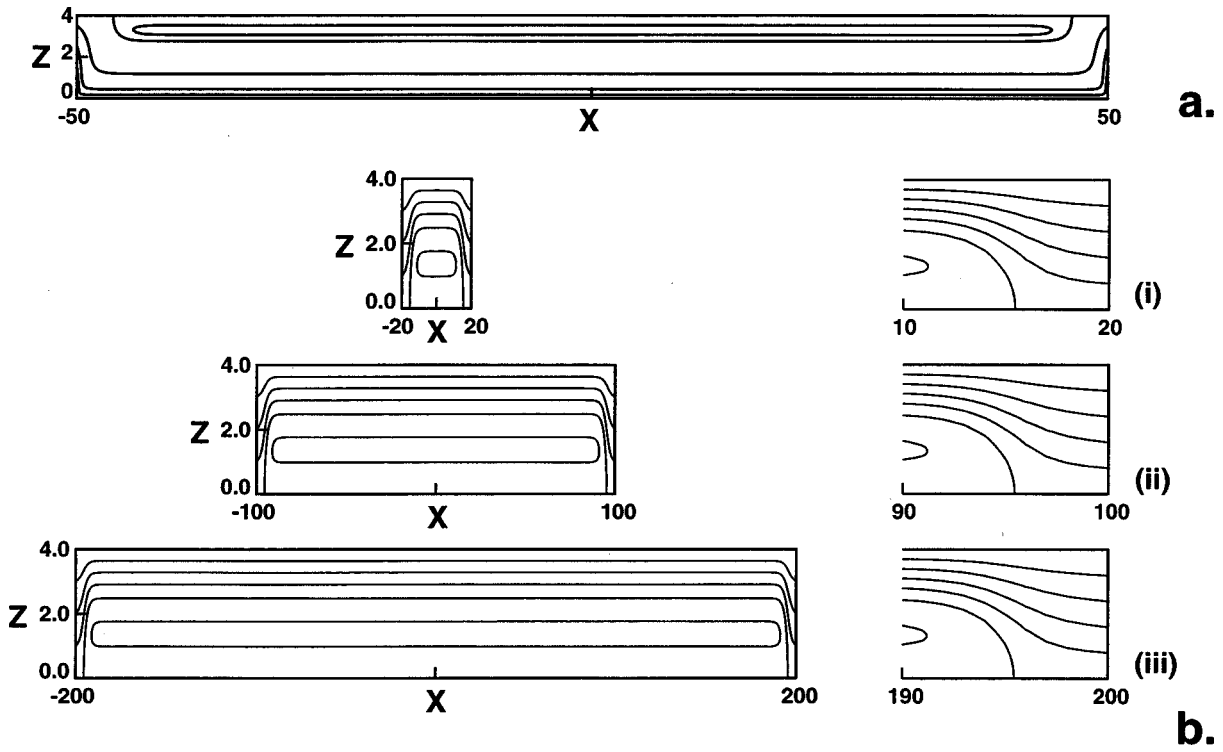

FIG. 5. Contour plots of the total streamfunction for representative examples of (a) a subcritical solitary wave of depression ($H=4$, $\Lambda=109.0$), and (b) upper branch solitary wave solutions ($H=4$, $\Lambda=0.981$) for a Boussinesq shear-free fluid with $\rho=\rho_0(1-\sigma\tanh(\psi))$. The width of the computational domain in the latter case is (i) $W=40$, (ii) $W=200$, (iii) $W=400$. An expanded portion of the flow domain which shows the detailed form of the streamline pattern near a lateral boundary is also illustrated for each of the upper branch solutions.

ously varying density profiles. An examination of the results presented by Pullin and Grimshaw indicates that the limiting ratio of wavelength, $\mathscr{W}_{1/2}$, to wave amplitude for interfacial waves is about 3.35, which is remarkably similar to our calculated result for a wave with amplitude $A=30$. Pullin and Grimshaw also find that the limiting interfacial wave occurs in the form of a stagnant bubble of fluid with a half-lens shape enclosed between two stagnation points at $x=\pm 2.18A$, $z=0$, where A is the wave amplitude. The coordinates of the stagnation points for the largest amplitude wave which we have calculated ($A=30$) are $x=\pm 1.87A$, $z=0$. These results suggest that the limiting large amplitude interfacial wave found by Pullin and Grimshaw is probably identical to the limiting large amplitude solitary wave in unbounded continuously stratified fluids. The difference between our results and those of Pullin and Grimshaw indicates that our largest amplitude wave has not quite reached the linear scaling regime. It can be anticipated that the morphology of very large amplitude waves in unbounded fluids will not depend on the density variation in a relatively thin pycnocline. Thus, we conclude that the limiting self-scaling solution for waves in unbounded continuously stratified fluids is identical to the limiting interfacial solution reported by Pullin and Grimshaw.

Additional evidence which indicates that large amplitude solitary waves in unbounded Boussinesq fluids differ in shape only by a scaling factor is provided by the laboratory observations described by Stamp and Jacka[17] of large amplitude deep fluid ($H=50$) mode-2 solitary waves. These authors also find that the wavelength of large amplitude waves appears to increase linearly with increasing amplitude and infer that the limiting ratio of wavelength to amplitude is about 4.2. This result is based on an extrapolation to very large amplitudes of results for waves with amplitudes between about 1.0 and 3.2. It is clear, however, from the theoretical curve presented in Fig. 7 that the true linear scaling regime exists only for waves with amplitudes greater than 30; the slope of the amplitude–wavelength curve varies significantly over the 1.0–3.2 amplitude range. Thus, the aspect ratio derived from the slope of the linear fit to the amplitude–wavelength data by Stamp and Jacka may not provide an accurate estimate of the true limiting ratio. Further remarks on the properties of large amplitude waves in unbounded fluids will be deferred until the end of Sec. III C.

B. Case 2: $\rho(\psi)=\rho_0(1-\sigma(1-e^{-\psi}))$

Here, we consider the properties of internal solitary waves in Boussinesq fluids with a Brunt–Väisälä frequency profile which varies exponentially with height. Again, we assume that $\rho(\psi)=\rho_0(1-\sigma F(\psi))$ is valid for all values of ψ. Although recirculation is once again a feature of larger amplitude waves, the amplitude–speed and amplitude–wavelength curves for flow models of this type reveal substantially different behavior from that found for waves in fluids with a hyperbolic tangent density profile.

The variation in amplitude with eigenvalue is plotted in Fig. 8 for solitary waves in Boussinesq fluids with total depths in the range from $H=1$ to $H=200$. Note that the unusual upper branch solitary wave solutions which were

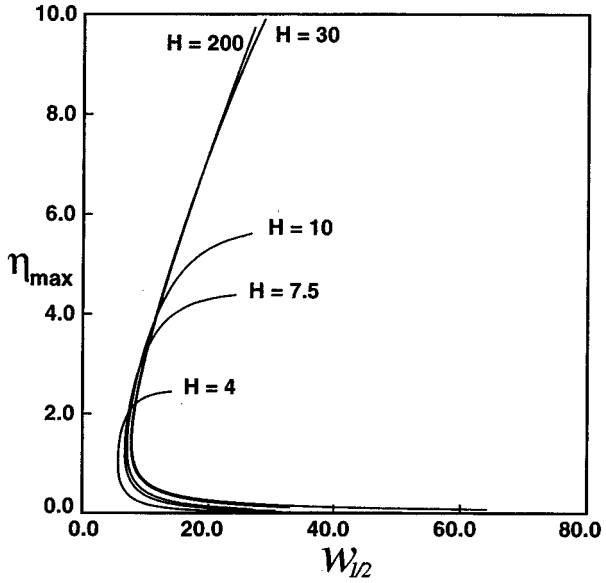

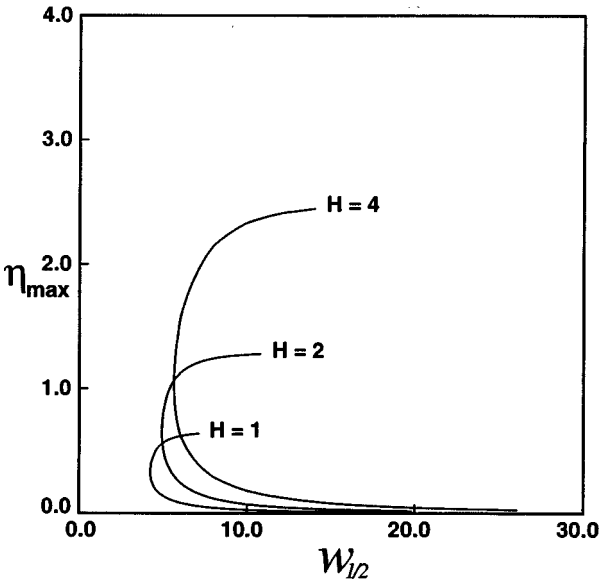

FIG. 6. Wave amplitude $\eta_{\max}$ vs wavelength $\mathscr{W}_{1/2}$ for solitary waves on the lower solution branches of the shear-free Boussinesq DJL equation for flow models with density $\rho(\psi)=\rho_0(1-\sigma\ \tanh(\psi))$. For the $H=1$ configuration the streamline corresponding to $\psi=0.5$ was used to determine the wavelength.

found for flow models with hyperbolic tangent density profiles apparently do not exist in fluids described by this flow model. The calculations indicate that, even in the case of unbounded fluids, the amplitude of the solitary wave solutions approaches a maximum value in the limit $\Lambda\rightarrow 0 (c\rightarrow\infty)$. This limiting amplitude is estimated to be about 0.88 for fluids with $H=1$ and 3.93 for fluids with $H=200$.

Figure 9 displays the variation in wavelength with amplitude for amplitudes ranging from relatively small values up to the limiting maximum amplitude for each flow model. Again, the results differ significantly from those found for flow models with hyperbolic tangent density profiles. In the case of shallow- and intermediate-depth fluid models, as wave amplitude increases, the wavelength decreases, even after the onset of closed circulation, to a minimum constant value. The deep fluid $H=200$ results differ in that the wavelength appears to increase slightly as the amplitude approaches the limiting maximum value. In essence, however, larger amplitude waves in this family are characterized by relatively narrow profiles.

TABLE II. Amplitude and wavelength of solitary waves with minimum wavelength and solitary waves at the onset of closed circulation, for waves in Boussinesq fluids with a hyperbolic tangent density profile. All quantities are nondimensional.

	Solitary wave with minimum wavelength		Solitary wave at onset of closed circulation	
H	$\eta_{\max}$	$\mathscr{W}_{1/2}$	$\eta_{\max}$	$\mathscr{W}_{1/2}$
1[a]	0.33	4.21	0.31	4.22
2	0.66	4.89	0.55	4.94
4	1.04	5.61	0.83	5.69
7.5	1.27	6.71	1.01	6.82
10.0	1.31	7.06	1.06	7.18
30.0	1.35	7.69	1.14	7.83
200.0	1.45	7.80	1.15	7.95

[a] $\psi=0.5$ streamline used to define wavelength when $H=1$.

The results presented here show that the properties of internal solitary waves in Boussinesq fluids with an exponential density profile are significantly different from those found for waves in fluids with a hyperbolic tangent density profile. In particular, as $\Lambda\rightarrow 0$, larger amplitude waves in this class approach a limiting wave profile with amplitude $\eta_{\max}\leqslant 3.93$ and a relatively small wavelength. Waves with arbitrarily large amplitudes do not exist in unbounded flow models of this type. The influence of further reductions in the eigenvalue on the properties of large amplitude waves appears only as an increase in wave speed and an increase in the degree of nonlinearity as manifested by increases in the fluid velocities in the interior of the wave. Further comments on the unusual properties of this flow model will be deferred to Sec. III D.

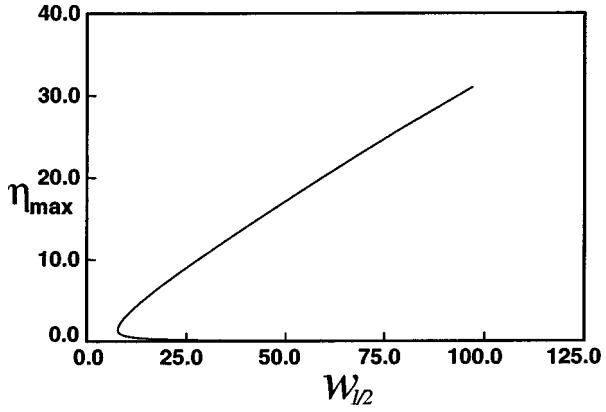

FIG. 7. Wave amplitude $\eta_{\max}$ plotted against wavelength $\mathscr{W}_{1/2}$ for very large amplitude solitary wave solutions to the Boussinesq shear-free DJL equation for a flow model with density $\rho(\psi)=\rho_0(1-\sigma\ \tanh(\psi))$ and nondimensional total fluid depth $H=200$.

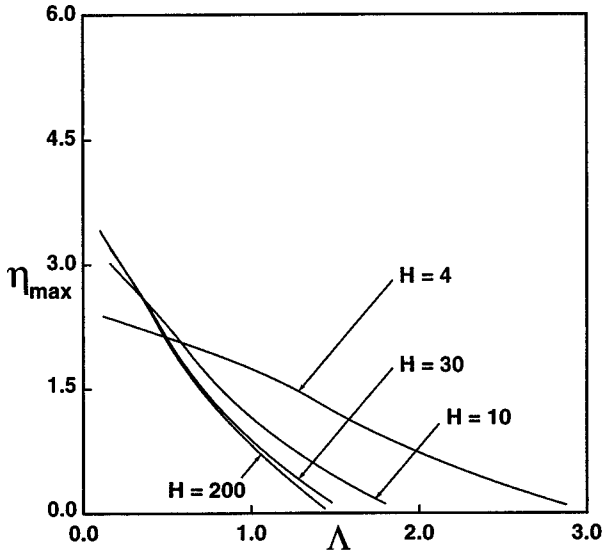

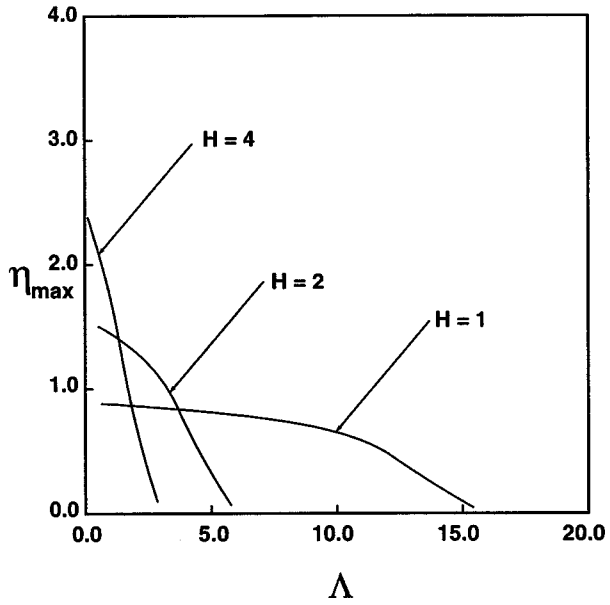

FIG. 8. Variation of wave amplitude $\eta_{\max}$ with eigenvalue Λ for solitary waves in flow models with density $\rho(\psi)=\rho_0(1-\sigma(1-e^{-\psi}))$.

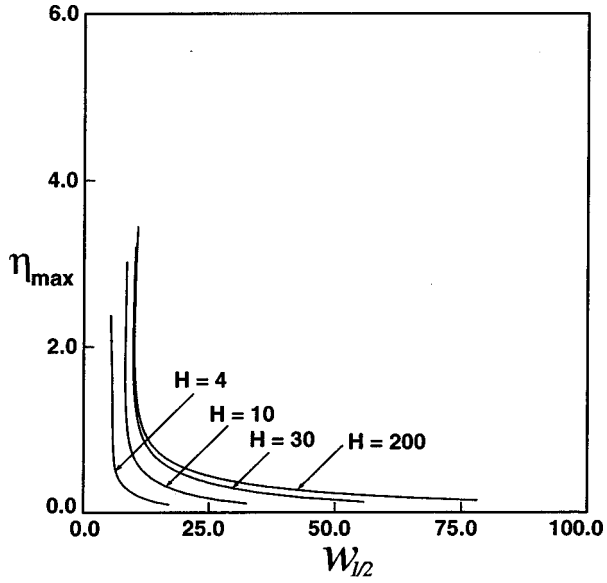

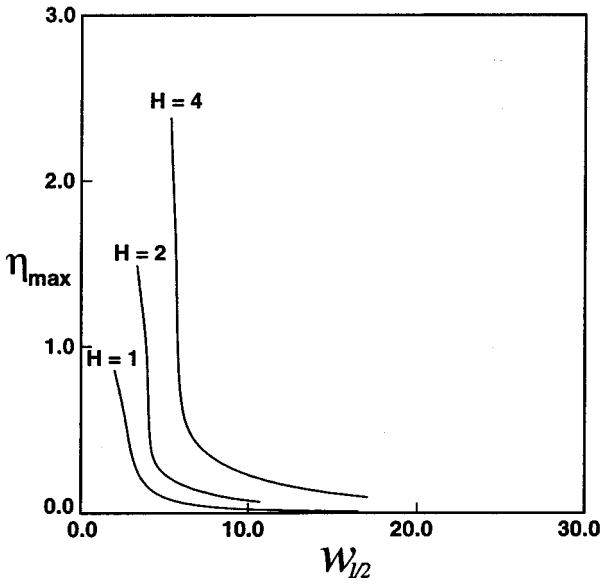

FIG. 9. Wave amplitude $\eta_{\max}$ as a function of wavelength $\mathscr{W}_{1/2}$ for solitary waves on the lower solution branches of the shear-free Boussinesq DJL equation for flow models with density $\rho(\psi)=\rho_0(1-\sigma(1-e^{-\psi}))$.

C. Case 3: $\rho(\psi)=\rho_0(1-\sigma(2/\pi)\arctan(\psi))$

The class of flow models studied in this section differs from the two classes considered above in that the ambient Brunt–Väisälä frequency decays algebraically with height. Plots of amplitude versus eigenvalue are presented in Fig. 10. The curves displayed in this diagram are qualitatively similar to the corresponding curves for the hyperbolic tangent density flow model. For fluids of finite depth, the eigenvalue decreases as wave amplitude increases from zero to a minimum value which is clearly marked by a discontinuity in the amplitude–eigenvalue curve. An upper solitary wave solution branch corresponding to waves with nonunique wavelength is present in all finite-depth flow models and large amplitude waves exhibit closed circulation in the streamline flow pattern. The calculated amplitude–wavelength curves are illustrated in Fig. 11. As in the case of hyperbolic tangent density flow models, wave broadening is found to be a characteristic of larger amplitude solitary waves in all flow models of this type. Although the calculations were not taken to extreme amplitudes, the results for the $H=200$ flow model in Fig. 11 suggest that, as in the case of a fluid with a hyperbolic tangent density profile, waves of large amplitude in unbounded fluids differ in form only by a scaling factor.

A comparison of the results presented here with those described above for flow models with hyperbolic tangent density profiles leads to two interesting conclusions. In the first place, we note that, for a given total fluid depth, the solitary wave amplitude at the limit point on the lower solution curve for waves in finite-depth fluids with hyperbolic tangent density profiles is identical, at least to within the accuracy of our calculations, to the amplitude of waves at the limit point in fluids with arctangent ambient density profiles. This suggests that the maximum amplitude of physically re-

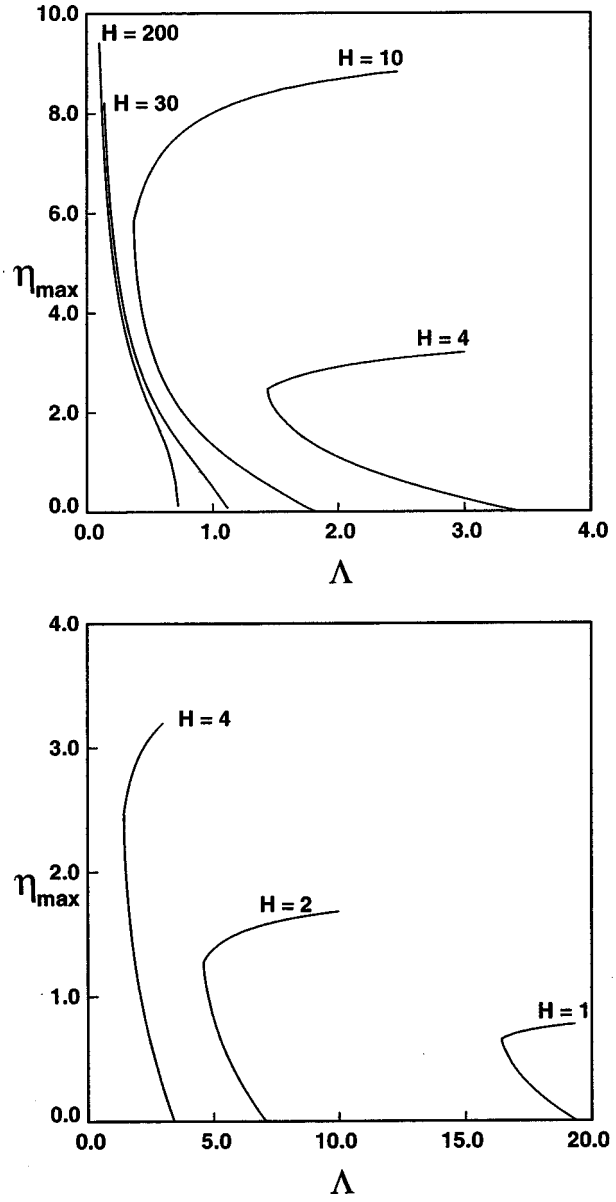

FIG. 10. Wave amplitude η_{max} vs eigenvalue Λ for solitary waves in flow models with density $\rho(\psi)=\rho_0(1-\sigma(2/\pi)\arctan(\psi))$.

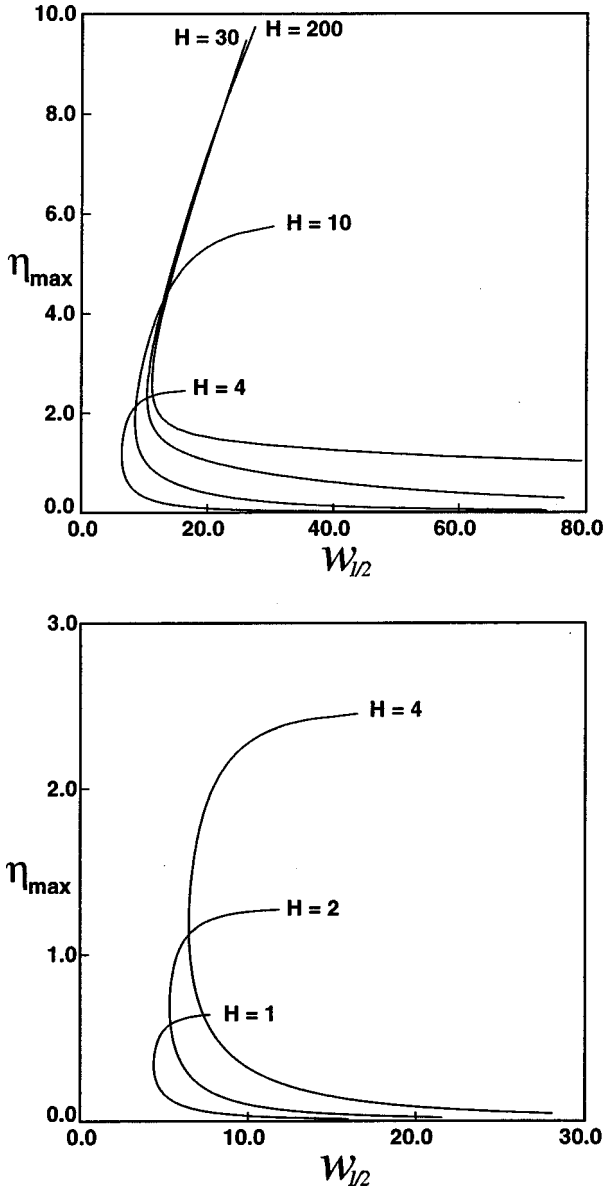

FIG. 11. Variation of wave amplitude η_{max} with wavelength $\mathscr{W}_{1/2}$ for solitary waves on the lower solution branches of the shear-free Boussinesq DJL equation for flow models with density $\rho(\psi)=\rho_0(1-\sigma(2/\pi)\arctan(\psi))$.

alistic internal solitary waves in finite-depth Boussinesq fluids may be independent of the detailed form of the fluid density profile, provided an upper solution branch exists. The second conclusion is based on the observation that the amplitude–eigenvalue and amplitude–wavelength curves for deep-fluid ($H=200$) flow models with hyperbolic tangent and arctangent density profiles appear to be identical in the limit of large wave amplitudes. Furthermore, as noted above, these very large amplitude deep-fluid solitary wave solutions appear to be nearly identical to the self-scaling very large amplitude interfacial wave solution discovered by Pullin and Grimshaw[3] in unbounded Boussinesq fluids. Thus, we conclude that, when a Boussinesq unbounded stratified fluid is capable of supporting solitary waves of unlimited amplitude, the properties of very large amplitude solitary waves are described by a single universal solution which does not depend on the form of the buoyancy profile. Indeed, it appears that this self-scaling solution is the same as the solution found by Kozlov and Makarov,[20] which describes mutually similar propagating intrusions in the form of a half-lens shaped body of denser stagnant fluid with stagnation points on the lower boundary at $x=\pm 2.16A$. It is worth noting as well that these limiting self-scaling disturbances appear to be identical to the limiting large amplitude form of the Pierrehumbert vortex.[21,22]

D. Case 4: $\rho(\psi)=\rho_0(1-\sigma\psi|(\psi+1))$

The final flow model considered here provides a second example of a flow configuration in which the Brunt–Väisälä frequency decays algebraically with increasing height. Our calculated results for the variation of amplitude with eigenvalue are presented in Fig. 12. Note that these curves have not been truncated at large amplitudes; the solution branches

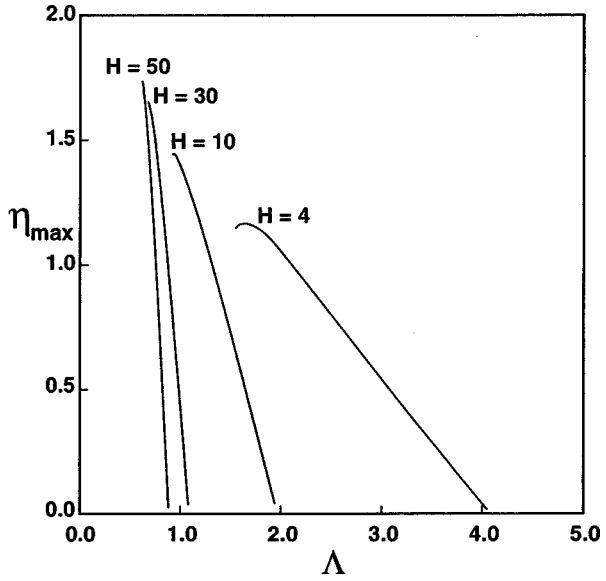

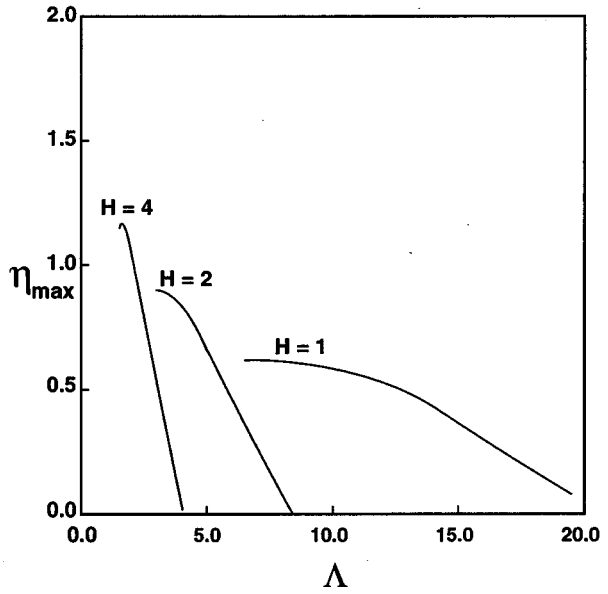

FIG. 12. Wave amplitude $\eta_{\max}$ plotted against eigenvalue Λ for solitary waves in flow models with density $\rho(\psi)=\rho_0(1-\sigma\psi/(\psi+1))$.

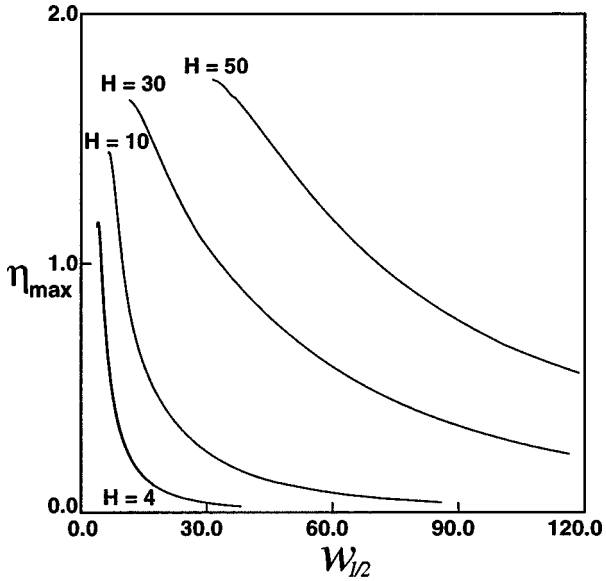

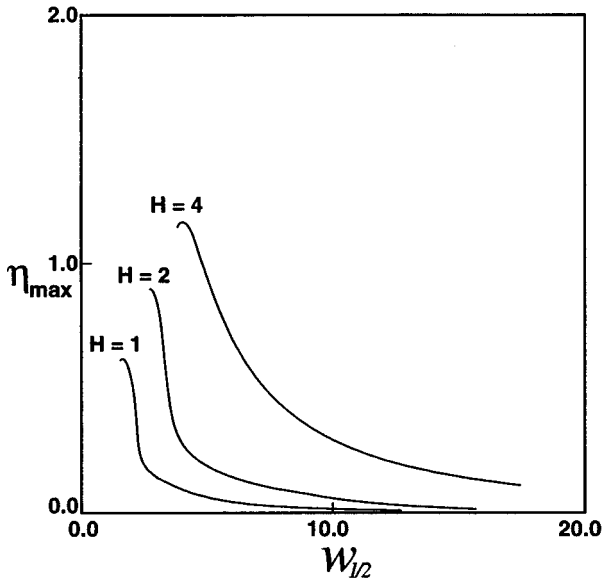

FIG. 13. Variation of wave amplitude, $\eta_{\max}$, with wavelength, $\mathscr{W}_{1/2}$, for solitary waves in shear-free fluids with density $\rho(\psi)=\rho_0(1-\sigma\psi/(\psi+1))$.

displayed in these diagrams extend to the minimum value of Λ and the maximum value of wave speed. No attempt has been made to determine the solution branches for fluids with depths greater than $H=50$ because the amplitude of waves in deep fluids varies rapidly with Λ and it has proven to be difficult to determine these deep fluid solution branches accurately.

An examination of the results presented here shows that the properties of internal solitary waves in fluids with $F(\psi)=\psi/(\psi+1)$ are fairly similar to the properties of the waves described above which propagate in fluids with exponential density profiles. Upper branch solutions corresponding to waves with nonunique wavelength do not exist in either of these flow configurations. The solutions found for the $F(\psi)=\psi/(\psi+1)$ flow models differ significantly, however, from those described above in Sec. III B in that a minimum value of Λ (and hence a maximum value of wave speed) exists for solitary waves in all flow models of this type. The results presented here also reveal another unexpected feature. In contrast with all other flow models, our calculations indicate that the wave of maximum amplitude in finite-depth fluids with $F(\psi)=\psi/(\psi+1)$ does not correspond to the wave with maximum speed. Instead, it appears that the wave of maximum speed has a slightly larger speed and a slightly smaller amplitude than the wave of maximum amplitude. This can be seen in the results presented in Fig. 12.

The variation in amplitude with wavelength for this particular ambient density profile is shown in Fig. 13. The behavior of waves in this flow model is similar to that found for waves in fluids with an exponential density profile in that wave broadening with increasing wave amplitude never occurs. Note, however, that the wave with minimum wavelength does not correspond to the wave with maximum amplitude; it corresponds instead to the wave with maximum speed at the point where the solution branch terminates.

IV. STRUCTURE OF LARGE AMPLITUDE WAVES WITH CLOSED CIRCULATION

We have shown that the properties of larger amplitude solitary wave solutions with closed circulation can differ radically from one flow model to another. At lower amplitudes, however, the characteristics of these solutions are similar for all flow models; wave speed increases and wavelength decreases with increasing amplitude as expected from weakly nonlinear theory. The large variation in wave properties which occurs after the onset of closed circulation suggests that the behavior of large amplitude waves can be explained, at least in part, by the density structure of the trapped recirculating fluid in regions where $\psi=\phi+z<0$. All of the calculations described above have been based on the assumption that the density streamfunction relation $\rho(\psi)=\rho_0(1-\sigma F(\psi))$ provides a valid description of the density variation inside recirculating flow regions bounded by $\psi=0$. That is, it has been assumed that the functional form of $F(\psi)$, which is valid for regions where the streamlines emanate from infinity, is also applicable to areas of the flow domain where $\psi<0$. The same assumption was used in the calculations reported by Davis and Acrivos[7] and Tung *et al.*[8] for large amplitude solitary wave solutions with recirculating flow. This procedure may not, however, provide a realistic description of the density structure in closed circulation cells which are bounded by $\psi=0$ since regions which are statically unstable appear in all large amplitude solutions whenever the horizontal particle speed exceeds the wave speed. An example of this statically unstable region is illustrated by the shaded area in Fig. 2(b).

It is clear that perfectly valid time-independent solitary wave solutions to the Dubreil-Jacotin–Long equation can be found with regions where $\rho(\psi)$ exceeds the density at the surface ρ_0. Even though these solutions are statically unstable they may possibly describe physically realistic solutions when the density throughout the closed circulation cell is only slightly larger than ρ_0. Thus, the large amplitude solutions described above for fluids with hyperbolic tangent or arctangent density profiles could possibly provide a reasonable description of physically realistic waves in Boussinesq fluids since the maximum variation in density in the trapped recirculating fluid is limited to $\Delta\rho=\sigma\rho_0$. It does not seem likely, however, that the larger amplitude solutions for fluids with either $F(\psi)=(1-e^{-\psi})$ or $F(\psi)=\psi/(\psi+1)$ can correspond to physically realizable waves. In both of these cases, the value of F increases without bound with increasingly negative values of ψ. The behavior of the curves displayed in Figs. 8 and 9 for fluids with $F(\psi)=(1-e^{-\psi})$ and in Figs. 12 and 13 for fluids with $F(\psi)=\psi/(\psi+1)$ can therefore be explained by noting that the solution curves terminate at relatively small maximum amplitudes when $F(\psi)\rightarrow-\infty$ in the limit $(\psi)\rightarrow-\infty$ for fluids with exponential density variation and in the limit $\psi\rightarrow-1.0$ for fluids with $\rho(\psi)=\rho_0(1-\sigma(\psi/(\psi+1)))$.

Several observations of the density distribution of recirculating fluid in large amplitude solitary waves have been reported. Clarke *et al.*,[23] in an experimental study of the Morning Glory of the Gulf of Carpentaria in northern Australia, found that recirculating fluid trapped in atmospheric solitary waves has the properties of undisturbed air ahead of the disturbance near the surface. The fluid distribution inside the well-documented atmospheric solitary wave described by Doviak and Christie[24] was slightly different. In this case, air which was slightly cooler (about 2 °C) than the air at the surface was observed at the center of the closed circulation cell. Similar observations have been reported by Cheung and Little[25] for highly nonlinear solitary waves in the nocturnal boundary layer. In this case, however, the density of the slightly cooler trapped fluid in the interior of the wave appears to be constant. Large amplitude solitary waves have also been observed in laboratory experiments with regions of trapped fluid with densities which are slightly larger than the density of the undisturbed fluid at the surface ahead of the wave (Davis and Acrivos;[7] Maxworthy;[16] Stamp and Jacka[17]). These observations suggest that solitary wave solutions with recirculating fluid densities which are constant or nearly constant and equal to or slightly higher than the density of the ambient fluid at the surface provide a reasonable description of physically realistic waves.

We will now examine briefly the characteristics of large amplitude solitary wave solutions to the Dubreil-Jacotin–Long equation which are nearly statically stable. These solutions differ from those described above in that the density streamfunction relation $\rho(\psi)=\rho_0(1-\sigma F(\psi))$ for a given flow configuration is defined separately for $\psi<0$ to ensure that the density of fluid in regions bounded by $\psi=0$ is only slightly larger than the ambient density at the surface, in agreement with laboratory and field observations of internal solitary waves.

Consider a fluid in which $F(\psi)=\psi/(\psi+1)$ when $\psi\geqslant 0$ and $F(\psi)=K\tanh(\psi)$ when $\psi<0$. Here, $K\sigma$, where $K\leqslant 1$, determines the maximum density in the recirculating fluid. The solutions to the Dubreil-Jacotin–Long equation in this case are identical to those found in Sec. III D for waves of modest amplitude with streamlines which are connected at every point in the flow field to the flow at infinity. At higher amplitudes when closed streamlines appear, the properties of the fluid inside the recirculation cell are determined by the same functional form for $F(\psi)$ as that used in Sec. III A for waves in fluids with a hyperbolic tangent density profile. Thus, since the maximum density variation in the closed circulation region is now restricted in the Boussinesq approximation to a small value, the solutions of the Dubreil-Jacotin–Long equation in this case should provide a fairly realistic description of internal waves of all amplitudes in fluids with ambient density $\rho(\psi)=\rho_0(1-\sigma(\psi/(\psi+1)))$. We note that the numerical calculations for this particular flow model are simplified by the fact that $F(\psi)$ and $F'(\psi)$ are continuous at $\psi=0$. $F''(\psi)$ is, however, not continuous at $\psi=0$.

Plots of amplitude versus eigenvalue and amplitude versus wavelength for this flow model are displayed in Figs. 14 and 15, respectively, for $K=1.0$. These results differ substantially from those shown in Figs. 12 and 13 for fluids with the same ambient density profile when the wave amplitude is large. In particular, an upper branch solution now exists for waves in finite-depth fluids, and there appears to be no upper limit to the amplitude of waves in unbounded fluids. These

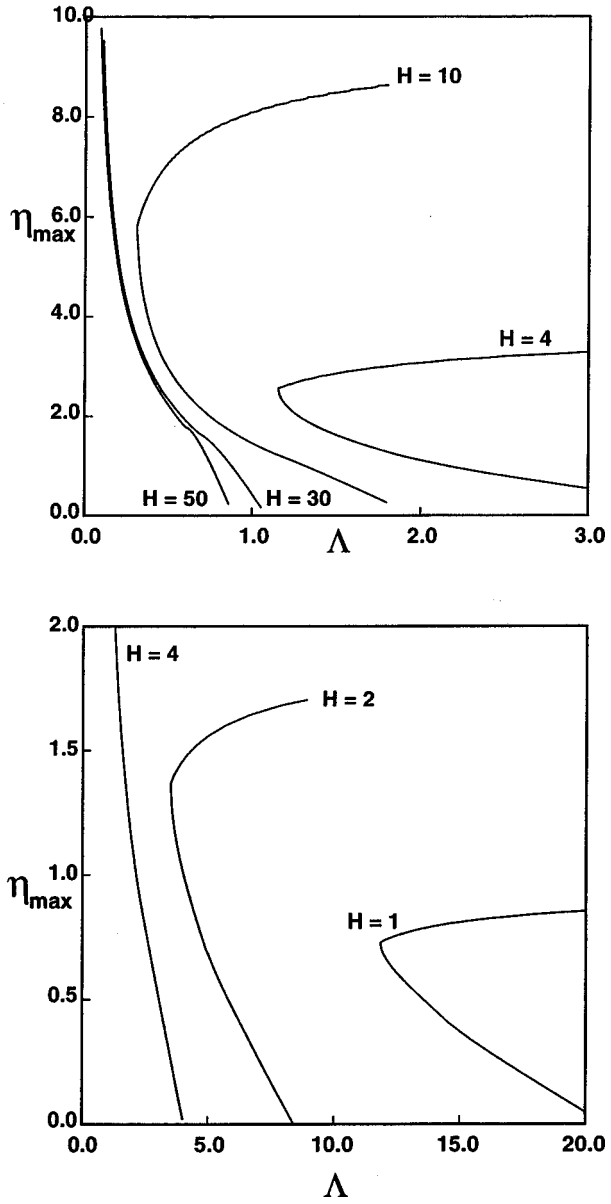

FIG. 14. Variation in wave amplitude η_{max} with eigenvalue Λ for solitary waves in flow models with $F(\psi)=\psi/(\psi+1)$, $\psi \geqslant 0$ and $F(\psi)=K\tanh(\psi)$, $\psi<0$ for $K=1.0$. The density of recirculating fluid in the interior of larger amplitude waves of this type is slightly larger than the undisturbed density at the surface ahead of the wave.

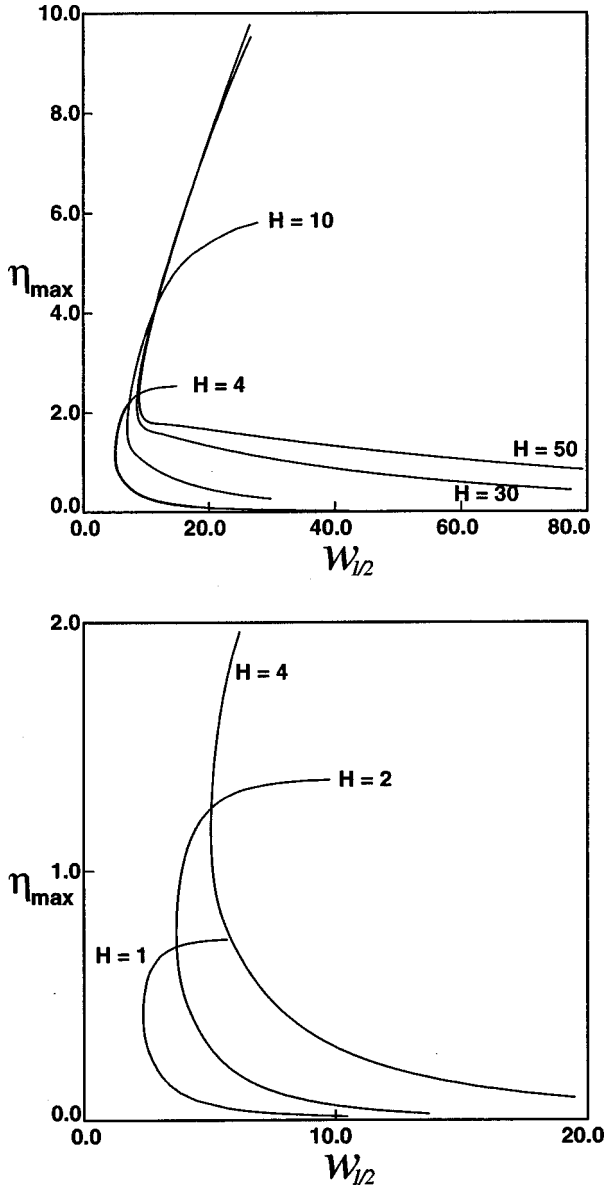

FIG. 15. Variation of wave amplitude, η_{max}, with wavelength, $\mathscr{W}_{1/2}$, for solitary waves in flow models with $F(\psi)=\psi/(\psi+1)$, $\psi \geqslant 0$ and $F(\psi)=K\tanh(\psi)$, $\psi<0$ for $K=1.0$.

results are, of course, identical to those described in Sec. III D for all solutions of modest amplitude. At higher amplitude, the behavior of the lower branch solution curves is similar to that found in Sec. III A for fluids with hyperbolic tangent density profiles. For fluids of finite depth, the wavelength decreases initially with increasing wave amplitude to a minimum value and then increases monotonically with further increases in wave amplitude until the lower solution branch terminates at the wave of maximum speed and amplitude. The behavior of waves in unbounded fluids is also similar in that a wave of minimum wavelength exists. These waves can have arbitrarily large amplitudes and they appear to approach the same limiting self-scaling solution as that found in Secs. III A and III C for waves in fluids with hyperbolic tangent and arctangent ambient density profiles. It is also worth noting that the limiting amplitude of the lower solution branch waves for a given total fluid depth appears to be slightly larger for shallow fluid flow configurations than the limiting amplitude found for both the hyperbolic tangent and arctangent density profile flow models. The wave speed at the limit point is again found to depend on the detailed form of the ambient density profile.

The numerical procedure which is used to solve the Dubreil-Jacotin–Long equation is not well-suited to calculations with flow models which have a discontinuity in $F'(\psi)$ at $\psi=0$. We have not, therefore, made an attempt to determine solutions for solitary waves which have regions of recirculating fluid with constant density. We believe, however, that physically realistic solutions of this type can be found by using a flow model in which the discontinuity in F' at $\psi=0$ is replaced with a suitably smooth function. The results

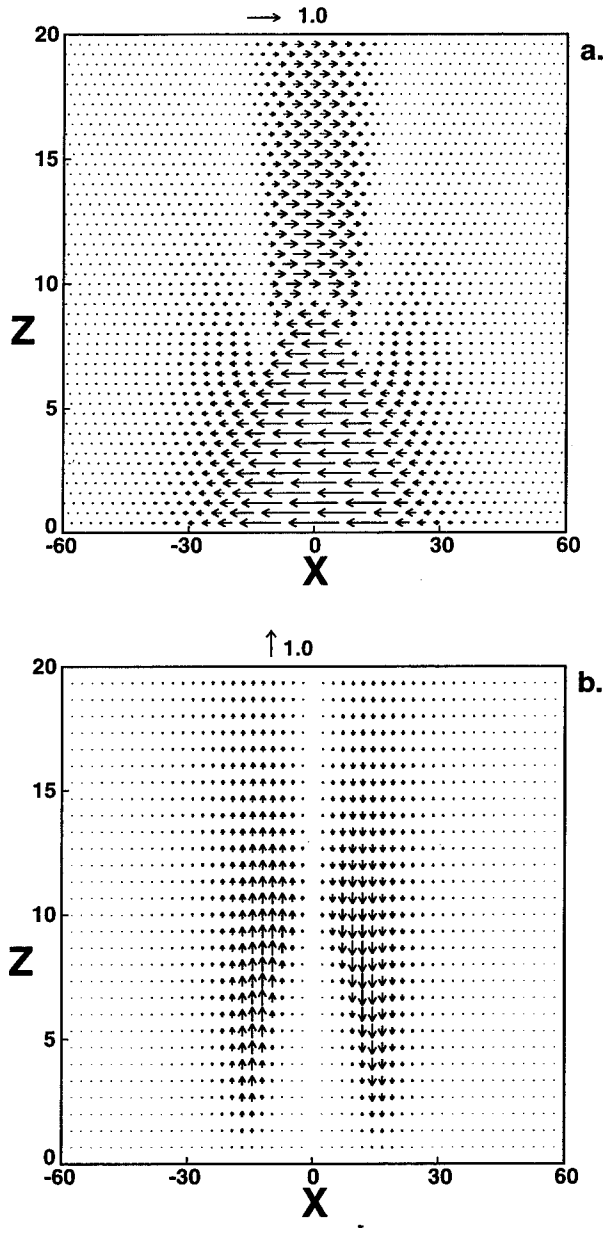

FIG. 16. The nondimensional fluid velocity components in an absolute frame of reference for a large amplitude ($a/h=9.7$) solitary wave propagating in a deep ($H=200$) shear-free Boussinesq fluid with density $\rho(\psi)=\rho_0(1-\sigma\tanh(\psi))$. The corresponding streamline pattern is illustrated in Fig. 2(b): (a) horizontal component; (b) vertical component.

presented here show that the morphology of large amplitude solitary waves with recirculating flow depends sensitively on the density distribution inside the closed circulation cell. This density distribution is determined by the functional form of $\rho(\psi)$ when $\psi<0$. We note as well, that the structure of large amplitude waves will also depend on the vorticity distribution inside the closed circulation cell. As with density, the vorticity of trapped recirculating fluid is influenced by the functional form of the horizontal shear, $U(\psi)$, when $\psi<0$. Calculations which include shear have been carried out for large amplitude solitary waves, but these results are beyond the scope of the present paper and will be described elsewhere.

V. FLUID VELOCITIES AND SURFACE PRESSURE

Field observations of atmospheric solitary waves are often based on observations of the surface wind and pressure. For atmospheric waves of relatively small amplitude, the surface wind and perturbation pressure signatures have the same form as the single-crested solitary wave streamline profiles predicted by weakly nonlinear wave theories.[26] The shape of these profiles (especially the surface perturbation pressure profile) may be substantially different for highly nonlinear waves with trapped recirculating fluid. The calculations presented here will be focused primarily on the morphology of the surface perturbation pressure signatures of highly nonlinear atmospheric solitary waves because solitary waves of large amplitude are frequently observed in the atmospheric boundary layer. Furthermore, the structure of the surface perturbation pressure signature provides a direct measure of the morphology of the closed circulation cell in highly nonlinear waves.

The relative fluid velocity components $\mathbf{u}_r=(u_r,w_r)$ can be calculated in a straightforward manner at any point in the flow field from the total streamfunction ψ by using

$$u_r=\frac{\partial\psi}{\partial z},\quad w_r=-\frac{\partial\psi}{\partial x}.$$

The absolute vertical velocity component w_a is, of course, identical to the relative vertical velocity component w_r and the absolute horizontal fluid velocity component, u_a, can be obtained by subtracting the wave speed c from u_r. An example of these calculations is presented in Fig. 16 for a very large amplitude solitary wave in a deep ($H=200$) fluid with a hyperbolic tangent density profile. These results correspond to the streamline pattern displayed in Fig. 2(b) and were carried out with $F(\psi)=\tanh(\psi)$, for both positive and negative values of ψ. An interesting feature of these results is the fine-scale structure in the horizontal velocity component in the region near the center of the wave at the top of the closed circulation cell. As noted above, the maximum density of the recirculating fluid in waves of this type is slightly higher than the density of the fluid at the surface ahead of the wave in the undisturbed flow. The area within the wave which is statically unstable corresponds to the shaded region shown in Fig. 2(b) where the horizontal fluid velocity component exceeds the wave speed c. The maximum fluid speed occurs at $z=0$ at the center of the wave. This maximum fluid speed is greater than the wave speed c when recirculating flow is present, but less than $2c$ for all deep fluid flow models considered here except in the case of the exponential density profile model described in Sec. III B. The latter case is exceptional (and physically unrealistic) because this flow model allows large densities in the core of the wave and very large gradients in the streamfunction and thus very large fluid velocity components in highly nonlinear waves, even in deep fluids. Similar calculations show that the maximum fluid speed in the center of the wave at the surface can easily exceed $2c$ in large amplitude waves which propagate in fluids of limited depth. These high values of the surface fluid speed have a significant influence on the surface pressure profile associated with solitary waves in finite-depth fluids.

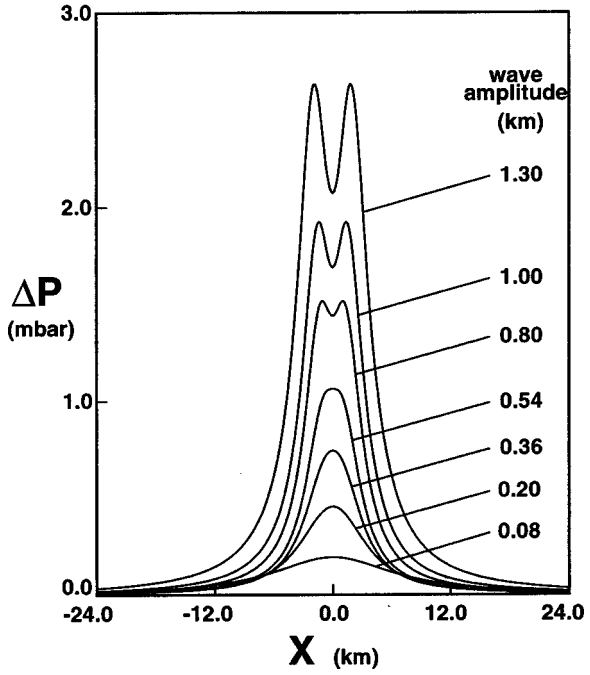

FIG. 17. The variation of surface perturbation pressure as a function of wave amplitude for solitary waves propagating in a deep ($H=100$), Boussinesq shear-free fluid with density $\rho(\psi)=\rho_0(1-\sigma\ \tanh(\psi))$. The effective depth of the waveguide is $h=500$ m, and $\rho_0=1.225$ kg/m^3.

Doviak and Christie[18] show that the surface perturbation pressure, p_s', associated with stationary nonlinear atmospheric wave motions can be written in terms of the perturbation wind speed at the surface, u', as

$$p_s'=\rho_0 u'\left[(c-u_0)-\frac{u'}{2}\right], \tag{7}$$

where u_0 is the ambient wind component at the surface in the direction of wave propagation and c is the speed of the wave. This expression for the surface perturbation pressure has the following interesting features when $u_0=0$ and $u'>0$:

(1) If the surface wind speed exceeds the wave propagation speed at some point in the flow by more than a factor of 2, then the perturbation pressure is negative; otherwise it is always positive.
(2) The surface perturbation pressure for solitary waves can have three extrema, one at the center of the disturbance where $(d/dx)|u|=0$ and, if $|u|>2c$, two at $u=+c$. These last two extrema correspond to the stagnation points in the relative streamline pattern at the surface and provide a precise measure of the horizontal dimension of the closed circulation cell.

Figure 17 shows the calculated surface perturbation pressure, p_s', for a sequence of finite-amplitude atmospheric boundary layer ($h=500$ m) solitary waves in a deep-fluid ($H=100$) shear-free Boussinesq flow model with $\rho(\psi)=\rho_0(1-\sigma\ \tanh(\psi))$ for all values of ψ. The bimodal surface pressure profiles indicate the presence of closed circulation in the relative streamline pattern, the horizontal extent of which is defined by the two maxima in p_s'. The surface perturbation pressure for these deep-fluid waves increases monotonically with wave amplitude and the amplitude of the pressure perturbation is always less than that predicted by first-order theory.

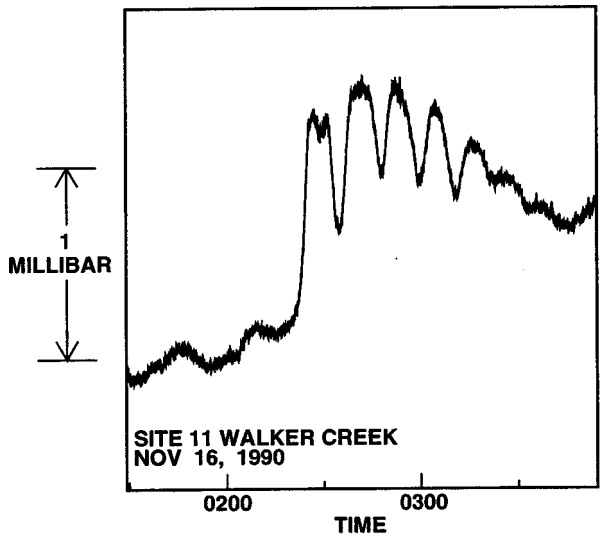

FIG. 18. Observed surface pressure record corresponding to an amplitude-ordered family of atmospheric solitary waves.

Bimodal solitary wave surface perturbation pressure signatures are commonly seen in field observations.[26] An example of a typical surface pressure record for an amplitude-ordered family of boundary-layer solitary waves observed over northern Australia is presented in Fig. 18. The pressure perturbation corresponding to the first solitary wave in this disturbance is clearly bimodal, which indicates the presence of a zone of recirculating fluid; the amplitudes of the following waves in this disturbance are apparently below the threshold for closed circulation.

We have also calculated the fluid velocity distributions and surface pressure perturbations of very large amplitude waves in a deep fluid near the large amplitude limit where wave profiles differ only by a scaling factor. An example of the surface perturbation pressure profile for $a/h=30$ is illustrated in Fig. 19. In this case, the surface fluid speed in the area between the two stagnation points is nearly constant and only slightly larger than the propagation speed, c, of the wave. We have not extended these calculations to waves of higher amplitude. The results suggest, however, that in the large amplitude limit, deep-fluid solitary waves in Boussinesq fluids exhibit a plateau-shaped surface perturbation pressure profile and contain an essentially stagnant region of trapped fluid.

As noted above, an interesting feature of solitary wave propagation in all finite-depth flow models is that the maximum horizontal wind speed at the surface can exceed twice the propagation speed of the wave when wave amplitudes are large. In this case the expression given in (8) shows that the surface perturbation pressure signature near the center of the wave will be negative. This is illustrated by the results presented in Fig. 20 which show the calculated surface perturbation pressure for a solitary wave propagating in a shallow Boussinesq flow configuration with $\rho(\psi)=\rho_0(1$

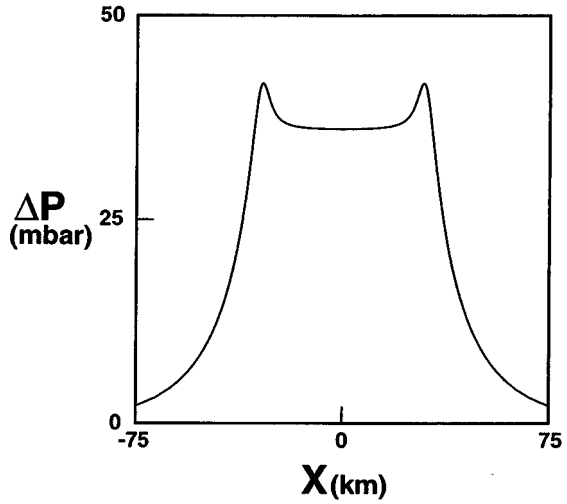

FIG. 19. Calculated surface perturbation pressure corresponding to a very large amplitude ($a/h=30$) solitary wave in a deep fluid ($H=100$) with density $\rho(\psi)=\rho_0(1-\sigma\ \tanh(\psi))$, $\rho_0=1.225\ \mathrm{kg/m^3}$, and $h=500$ m.

$-\sigma\tanh(\psi)$) for all values of ψ. The surface perturbation pressure signature for this highly nonlinear shallow-fluid wave bears little resemblance to the single-crested profile predicted by weakly nonlinear theory. This can lead to complications in the interpretation of surface observations of the pressure signature of atmospheric solitary waves which propagate in effectively shallow-fluid waveguides such as those which are created by the presence of an elevated critical layer.[27] Since the value of the surface perturbation pressure associated with solitary waves in shallow fluids may be close to zero at the center of the wave, one might be led to conclude from the observed surface pressure signature generated by a single wave of this type that the observations correspond to two solitary waves. Alternatively, the negative pressure dip at the center of the surface pressure signature might be much more pronounced than that illustrated in Fig. 20. In this case, the observed wave might be incorrectly identified as a solitary wave of depression.

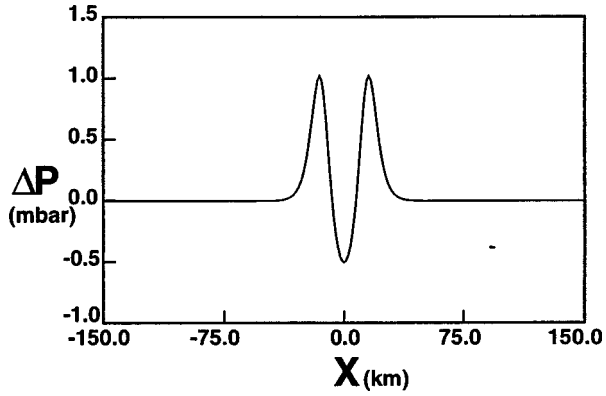

FIG. 20. Calculated surface perturbation pressure signature for a solitary wave propagating in a shallow fluid ($H=1$) with density $\rho(\psi)=\rho_0(1-\sigma\ \tanh(\psi))$. Here, $\rho_0=1.225\ \mathrm{kg/m^3}$, the effective depth is $h=5000$ m, and $a/h=0.7$.

VI. SUMMARY AND DISCUSSION

It has been shown in this study that the characteristics of finite-amplitude internal solitary waves in Boussinesq fluids depend sensitively on the form of the ambient stability profile. In the case of finite-depth flow models in which the density is given by either $\rho(\psi)=\rho_0(1-\sigma\ \tanh(\psi))$ or $\rho(\psi)=\rho_0(1-\sigma(2/\pi)\ \arctan(\psi))$ for both positive and negative values of ψ, an internal solitary wave of maximum amplitude exists. Since the wave of maximum amplitude corresponds to a minimum in the eigenvalue, this wave is also the wave of maximum speed. We have found that the maximum amplitude of waves in these two types of flow models appear to be identical for flow configurations of the same depth. The wave speed for these limiting finite-depth solutions does, however, depend on the form of the density profile. Similar results have been found for a flow model with $F(\psi)=\psi/(\psi+1)$, $\psi>0$ and with the density in the recirculating flow region ($\psi<0$) restricted to values which are at most only slightly larger than the value of the ambient density at the surface. These results differ, however, in the case of shallow fluids where the maximum amplitude of waves on the lower branch is slightly larger than the value found for flow models in which $\rho(\psi)$ has the same functional form for both positive and negative values of ψ. These results suggest that the maximum amplitude of physically acceptable internal solitary waves in all finite-depth Boussinesq fluids may be independent of the ambient density profile when $\rho(\psi)$ is analytic for all ψ. An important outcome of this work is that it is clear that when recirculation occurs the morphology of solitary waves is strongly influenced by the density structure and vorticity distribution inside the closed circulation cell. The properties of the trapped recirculating fluid inside large amplitude waves are not determined *a priori* by the density and shear profiles in the ambient fluid.

In all cases where $|F(\psi)|$ is bounded when $\psi<0$, waves in deep fluids appear to exist with arbitrarily large amplitudes. The profiles of these large amplitude waves differ only by a scaling factor. In addition, the calculations described here, which are necessarily limited, suggest that the limiting solution for very large amplitude internal solitary waves in unbounded fluids is independent of the ambient density profile. These self-scaling large amplitude disturbances appear to be identical to the limiting large amplitude mutually similar form of the Pierrehumbert vortex.

The upper branch solutions, previously noted by Tung *et al.*[8] have been found to be computational domain-width dependent with arbitrary wavelengths and have been shown to extend from a supercritical eigenvalue to indefinitely large eigenvalues in the subcritical regime. These upper branch solitary wave solutions, therefore, do not appear to correspond to physically realistic waves. Upper branch solutions have also been determined for other flow models in which $\rho(\psi)$ remains bounded in the limit $\psi\to-\infty$. If this condition is not satisfied, the lower solution branch terminates at relatively small amplitudes and the upper branch solutions do not appear to exist. A new solitary wave solution branch which describes subcritical waves of depression has also been found. The calculations show, however, that these

waves also have arbitrary wavelengths and therefore do not appear to correspond to physically realistic waves.

Notable departures from the predictions of weakly nonlinear theory were observed. Wave broadening occurs at higher amplitudes for physically realistic solitary waves for all flow models considered here which have both lower and upper branch solutions. In contrast, for flow models which exhibit only lower branch solutions, the wavelength decreases monotonically to a minimum (nonzero) value corresponding to the wave of maximum speed.

A bimodal surface perturbation pressure signature is found to be a feature of larger amplitude waves. This signature provides a direct measure of the horizontal extent of the closed circulation cell in large amplitude waves. In the case of finite-depth fluids, the trough in the center of the pressure distribution may be so pronounced in highly nonlinear waves that the perturbation pressure becomes negative. These results can be used to interpret observations of surface pressure signatures of atmospheric solitary waves.

ACKNOWLEDGMENTS

This work was supported in part by the Universities Space Research Association under Contract No. NAS5-32484. Some of the work reported in this paper was carried out while D.J.B. was a Visiting Scientist at the Goddard Spaceflight Center, Greenbelt, MD. The authors would like to thank Professor Roger Grimshaw for a number of helpful comments and suggestions, and Dr. Frank de Hoog for providing some insight into the numerics of this particular problem. Most of the calculations presented in this paper were carried out on the Fujitsu VP2200 of the Australian National University's Supercomputer Facility.

APPENDIX: NUMERICAL SOLUTION OF THE DUBREIL-JACOTIN–LONG EQUATION

We wish to find numerical solutions to Eq. (3) subject to the boundary conditions (4)–(6). We shall first consider the small-amplitude limit for which the DJL equation takes the approximate linear form

$$(\nabla^2+\Lambda F'(z))\,\phi=0. \tag{A1}$$

Solutions to Eq. (A1) are the steady-state solutions to the time-dependent problem

$$\frac{\partial\phi}{\partial t}-(\nabla^2+\Lambda F'(z))\,\phi=0, \tag{A2}$$

and take the general form $\phi(x,z,t)=\exp\{t(\nabla^2+\Lambda F'(z))\}A(x,z)$, for some initial starting value $A(x,z)$.

The steady-state solution, ϕ_0, is the solution of interest and is determined by the limit

$$\lim_{t\to\infty}\phi(x,z,t)=\lim_{t\to\infty}[\exp\{t(\nabla^2+\Lambda F'(z))\}A(x,z)]$$

$$=\begin{cases}0 & \text{if } \Lambda<\Lambda_0\\ \phi_0 & \text{if } \Lambda=\Lambda_0,\\ -\infty & \text{if } \Lambda>\Lambda_0\end{cases}$$

where

$$\nabla^2\phi_0+\Lambda_0F'(z)\,\phi_0=0.$$

By implementing this limit procedure numerically, it is possible to arrive at a steady-state solution to Eq. (A2), and hence (A1). Although a rigorous mathematical proof is beyond the present authors, this technique can also be used to solve the fully-nonlinear problem

$$\frac{\partial\phi}{\partial t}-(\nabla^2+\Lambda F'(\phi+z))\,\phi=0, \tag{A3}$$

the problem of interest.

First, one discretizes Eq. (A3). In the present study, a simple forward-time-centered-space (FTCS) finite-difference procedure was used. One chooses a starting eigenfunction $\phi^{(0)}$, which can be taken from weakly nonlinear theory, and an eigenvalue $\Lambda^{(0)}$ as an initial ''guess.'' The algorithm is then allowed to evolve. If the algorithm converges to the zero solution, we can deduce that $\Lambda^{(0)}$ is too small. Conversely, if it diverges (or converges to an upper branch solution) then we know that $\Lambda^{(0)}$ was too large. Thus, by employing a binary-chop procedure on the eigenvalue, successive better trials $\Lambda^{(1)},\Lambda^{(2)},\ldots$, are obtained. The sequence $\{\Lambda^{(n)}\}$ converges to an eigenvalue which solves the problem. This numerical procedure is capable of determining solutions of arbitrary accuracy, and it never fails to converge. For a 100×100 finite-difference mesh, for well-posed problems, machine-level accuracy is achieved for each eigenfunction in around 0.25 s when run on a Fujitsu VP2200 supercomputer.

[1] L. A. Ostrovsky and Yu. A. Stepanyants, ''Do internal solitons exist in the oceans?'' Rev. Geophys. **27**, 293 (1989).
[2] D. R. Christie, ''The Morning Glory of the Gulf of Carpentaria: A paradigm for nonlinear waves in the lower atmosphere,'' Aust. Meteor. Mag. **41**, 21 (1992).
[3] D. I. Pullin and R. H. J. Grimshaw, ''Finite-amplitude solitary waves at the interface between two homogeneous fluids,'' Phys. Fluids **31**, 3550 (1988).
[4] L. K. Forbes and S. R. Belward, ''Atmospheric interfacial waves,'' Phys. Fluids A **4**, 2222 (1992).
[5] M. K. Dubreil-Jacotin, ''Sur les théoremes d'existence relatifs aux ondes permanentes périodiques à deux dimensions dans les liquides hétérogènes,'' J. Math. Pures Appl. **16**, 43 (1937).
[6] R. R. Long, ''Some aspects of the flow of stratified fluids. I. A theoretical investigation,'' Tellus **5**, 42 (1953).
[7] R. E. Davis and A. Acrivos, ''Solitary internal waves in deep water,'' J. Fluid Mech. **29**, 591 (1967).
[8] K. K. Tung, T. F. Chan, and T. Kubota, ''Large amplitude internal waves of permanent form,'' Stud. Appl. Math. **65**, 1 (1982).
[9] B. Turkington, A. Eydeland, and S. Wang, ''A computational method for solitary internal waves in a continuously stratified fluid,'' Stud. Appl. Math. **85**, 93 (1991).
[10] J. M. Vanden-Broeck and R. E. L. Turner, ''Long periodic internal waves,'' Phys. Fluids A **4**, 1929 (1992).
[11] D. J. Benney and D. R. S. Ko, ''The propagation of long large amplitude internal waves,'' Stud. Appl. Math. **59**, 187 (1978).
[12] D. J. Benney and R. Grimshaw, ''Large amplitude solitary waves in unbounded stratified fluids,'' Stud. Appl. Math. **66**, 181 (1982).
[13] O. G. Derzho and M. G. Velarde, ''Solitary waves of permanent form in a deep fluid with weak shear,'' Phys. Fluids **7**, 1357 (1995).
[14] O. G. Derzho and R. Grimshaw, ''Solitary waves with a vortex core in a shallow layer of stratified fluid,'' Phys. Fluids **9**, 1378 (1997).
[15] T. B. Benjamin, ''Internal waves of finite amplitude and permanent form,'' J. Fluid Mech. **25**, 241 (1966).
[16] T. Maxworthy, ''On the formation of nonlinear internal waves from gravi-

tational collapse of mixed regions in two and three dimensions,'' J. Fluid Mech. **96**, 47 (1980).
[17]A. P. Stamp and M. Jacka, ''Deep-water internal solitary waves,'' J. Fluid Mech. **305**, 347 (1995).
[18]R. J. Doviak and D. R. Christie, ''*Buoyancy wave hazards to aviation*,'' Proceedings of the Fourth International Conference on Aviation Weather Systems, Paris (Amer. Meteor. Soc., 1991), pp. 247–252.
[19]G. K. Batchelor, ''On steady laminar flow with closed streamlines at large Reynolds number,'' J. Fluid Mech. **1**, 177 (1956).
[20]V. F. Kozlov and V. G. Makarov, ''A category of steady-state gravity currents with a density discontinuity,'' Izv., Acad. Sci., USSR, Atmos. Oceanic Phys. **26**, 293 (1990).
[21]R. T. Pierrehumbert, ''A family of steady, translating vortex pairs with distributed vorticity,'' J. Fluid Mech. **99**, 129 (1980).
[22]P. G. Saffman and S. Tanveer, ''The touching pair of equal and opposite uniform vortices,'' Phys. Fluids **25**, 1929 (1982).
[23]R. H. Clarke, R. K. Smith, and D. G. Reid, ''The Morning Glory of the Gulf of Carpentaria: An atmospheric undular bore,'' Mon. Weather Rev. **109**, 1726 (1981).
[24]R. J. Doviak and D. R. Christie, ''Thunderstorm-generated solitary waves: A wind shear hazard,'' J. Aircr. **26**, 423 (1989).
[25]T. K. Cheung and C. G. Little, ''Meteorological tower, microbarograph array and sodar observations of solitary-like waves in the nocturnal boundary layer,'' J. Atmos. Sci. **47**, 2516 (1990).
[26]D. R. Christie, ''Long nonlinear waves in the lower atmosphere,'' J. Atmos. Sci. **11**, 1462 (1989).
[27]E. D. Skyllingstad, ''Critical layer effects on atmospheric solitary and cnoidal waves,'' J. Atmos. Sci. **48**, 1613 (1991).